*remote sensing*

MDPI

*Review*

# Quantification of Microtopography in Natural Ecosystems Using Close-Range Remote Sensing

**Tarini Shukla [1,2,*], Wenwu Tang [2,3,4], Carl C. Trettin [5], Gang Chen [4,6], Shenen Chen [1] and Craig Allan [4]**

1 Department of Civil and Environmental Engineering, University of North Carolina at Charlotte, Charlotte, NC 28223, USA
2 Center for Applied Geographic Information Science (CAGIS), University of North Carolina at Charlotte, Charlotte, NC 28223, USA
3 School of Data Science, University of North Carolina at Charlotte, Charlotte, NC 28223, USA
4 Department of Geography and Earth Sciences, University of North Carolina at Charlotte, Charlotte, NC 28223, USA
5 Center for Forested Wetlands Research, USDA Forest Service, Cordesville, SC 29434, USA
6 Laboratory for Remote Sensing and Environmental Change (LRSEC), Department of Geography and Earth Sciences, University of North Carolina at Charlotte, Charlotte, NC 28223, USA
* Correspondence: tshukla@uncc.edu

**Abstract:** Microtopography plays an important role in various ecological, hydrologic, and biogeochemical processes. However, quantifying the characteristics of microtopography represents a data-intensive challenge. Over the last decade, high-resolution or close-range remote sensing data and techniques have emerged as powerful tools to quantify microtopography. Traditional field surveys were mostly limited to transects or small plots, using limited sets of observations but with the decrease in the cost of close-range remote sensing technologies and the increase in computing performance, the microtopography even in forested environments can be assessed. The main objective of this article is to provide a systematic framework for microtopographic studies using close-range remote sensing technologies. This is achieved by reviewing the application of close-range remote sensing to capture microtopography and develop microtopographic models in natural ecosystems. Specifically, to achieve the main objectives, we focus on addressing the following questions: (1) What terrain attributes represent microtopography in natural ecosystems? (2) What spatial resolution of terrain attributes is needed to represent the microtopography? (3) What methodologies have been adopted to collect data at selected resolutions? (4) How to assess microtopography? Current research, challenges, and applicability of close-range remote sensing techniques in different terrains are analyzed with an eye to enhancing the use of these new technologies. We highlight the importance of using a high-resolution DEM (less than 1 $m^2$ spatial resolution) to delineate microtopography. Such a high-resolution DEM can be generated using close-range remote sensing techniques. We also illustrate the need to move beyond elevation and include terrain attributes, such as slope, aspect, terrain wetness index, ruggedness, flow accumulation, and flow path, and assess their role in influencing biogeochemical processes such as greenhouse gas emissions, species distribution, and biodiversity. To assess microtopography in terms of physical characteristics, several methods can be adopted, such as threshold-based classification, mechanistically-based delineation, and machine learning-based delineation of microtopography. The microtopographic features can be analyzed based on physical characteristics such as area, volume, depth, and perimeter, or by using landscape metrics to compare the classified microtopographic features. Remote sensing techniques, when used in conjunction with field experiments/data, provide new avenues for researchers in understanding ecological functions such as biodiversity and species distribution, hydrological processes, greenhouse gas emissions, and the environmental factors that influence those parameters. To our knowledge, this article provides a comprehensive and detailed review of microtopography data acquisition and quantification for natural ecosystem studies.

**Keywords:** microtopography; high-resolution; LiDAR; unmanned aerial system; remote sensing

check for updates

**Citation:** Shukla, T.; Tang, W.; Trettin, C.C.; Chen, G.; Chen, S.; Allan, C. Quantification of Microtopography in Natural Ecosystems Using Close-Range Remote Sensing. *Remote Sens.* **2023**, *15*, 2387. https://doi.org/10.3390/rs15092387

Academic Editors: Carlos Alberto Silva and Balázs Székely

Received: 27 January 2023
Revised: 25 April 2023
Accepted: 28 April 2023
Published: 2 May 2023

**Copyright:** © 2023 by the authors. Licensee MDPI, Basel, Switzerland. This article is an open access article distributed under the terms and conditions of the Creative Commons Attribution (CC BY) license (https://creativecommons.org/licenses/by/4.0/).

## 1. Introduction

The spatial heterogeneity of microtopography, where elevation differences are often less than a meter, plays a significant role in various ecological, hydrologic, and biogeochemical processes including carbon (C) and nitrogen (N) dynamics [1–4]. The biogeochemical importance of microtopography lies in its impact on carbon sequestration [5,6], greenhouse gas (GHG) emissions, and other biogeochemical processes [7–9], and hydrological function [10,11]. These processes or functions are influenced by surface microtopography [12–15]. For example, in an estuarine environment, the tidal riparian zone is affected by the interaction of microtopography and daily tidal fluctuations, which results in a complex pattern of soil gas emissions [16]. The biogeochemical activity, soil characteristics, and spatial interactions between vegetation, nutrients, hydrology, microbial communities, and soil organic carbon are all in part influenced by microtopographic features [17–19]. Microtopography also explains vegetation composition in wetlands and forests due in part to vertical variations in soil water, which impact the availability of nutrients such as phosphate and ammonium [12]. In addition, the spatial and temporal distributions of hydrologic connectivity in forested wetland landscapes can be substantially influenced by microtopography. The microtopography can be categorized into microtopographic features, as in the case of forested wetlands, which are characterized by hummocks or mounds (local high points), hollows or depressions (local low points), and lawns (intermediate elevation points). Hummocks are higher elevation patches in a wetland consisting of dense mats of soil, moss, and roots from herbaceous vegetation, while hollows are found at a comparatively lower elevation where the soil is saturated.

### *1.1. Defining Microtopography*

To understand the ecological, hydrologic, and biogeochemical processes from a micro to macro (or local to global) scale, it is important to quantify microtopography and identify the scale of a high-resolution model which can appropriately represent the spatial heterogeneity of the study site. It is vital to first define microtopography and microtopographic features in order to quantify and classify spatially heterogeneous topography in natural ecosystems. Hunneke and Sharitz [20] defined microtopography as spatial heterogeneity at the scale of plants and individual seeds. Along a similar vein, Titus [21], Bledsoe, and Shear [22] stated microtopography is the elevation or topographic heterogeneity of substrates at the scale of individual plants where the elevation ranges from 1 cm to 1 m. Subsequently, Moser et al. [23] described microtopography as the combination of relief and roughness where relief is vertical variation and roughness represents topographical variability. Diamond et al. [24] and Stovall et al. [25] referred to microtopography as the vertical variation in the ground surface occurring at centimeter to meter scales. Although elevation is the most common terrain attribute associated with microtopography, other terrain attributes such as slope, aspect, flow path, ruggedness index, wetness index, and curvature can also be significant in microtopography-based studies [26].

Microtopography, which influences ecological, hydrological, and/or biogeochemical processes, can be defined and classified irrespective of the spatial extent of a study area, which means it can range from individual soil cores and field plots to the scale of a watershed. In addition, microtopographic features are not limited to hummocks and hollows (common microtopographic features in wetlands) or pits and mounds (microtopographic features in forests). Instead, microtopographic features are the landscape characteristics that are classified and/or delineated based on their spatial and temporal extent to estimate the impact of microtopography on ecosystem functions. In summary, microtopography represents the variation in terrain elevation observed at a small (e.g., sub-meter) spatial scale over a study site, and the microtopographic features are the landscape characteristics that can be delineated based on terrain attributes over a given spatial and temporal extent.

### *1.2. Microtopography Influences Ecosystem Processes*

Small-scale variations in microtopographic features when studied over a large extent may exert significant impacts on hydrologic, biogeochemical, and biologic processes. In natural ecosystems, microtopography influences the hydroperiodicity in hollows, hummocks, and soil moisture, which in turn impacts element cycling. The surface flow path is greatly influenced by the spatial arrangement of hollows and hummocks where hummocks can reduce the water storage by up to 30% [27]. Assuming a homogeneous surface without considering microtopography can alter the surface water flow in a modeling exercise and, in turn, the associated results. Based on soil saturation, the hollows become the local control point for methane emissions, and over a large extent can be considered as ecosystem control points. In contrast, hummocks are often the control points for high primary productivity. Multiple studies [4,28,29] have shown that there is spatial variation in wetlands' $CO_2$ and $CH_4$ emissions; hollows with a reduced redox state (low oxygen availability) are the source of greater methane emissions. Due to extended exposure to open air and availability of nutrients, hummocks are the source of carbon dioxide emissions.

Microtopography also influences exogenous processes such as landslides, erosion, and nutrient transportation. Exogenous processes are the result of the interaction between geological, hydrological, and meteorological factors and microtopography. Processes such as soil erosion and runoff have a significant role in sediment/nutrient transportation. Studies [26,30,31] conducted at a fine spatial scale showed the importance of microtopography in studying exogenous processes.

### *1.3. Microtopography with Close-Range Remote Sensing*

Recent studies have reported the use of close-range remote sensing technologies to map fine-scale microtopography by using dense and highly accurate elevation data over reasonably large areas [25,32–35]. However, this is a recent development, and researchers examining fine-scale processes or distributions have traditionally relied on labor-intensive manual field surveys. It is our view that a more complete understanding of the state-of-the-art remote sensing techniques and their limitations will facilitate their incorporation into future experimental designs and modeling applications examining such topics as carbon cycling, hydrologic processes, and vegetation pattern and composition at fine spatial scales. The aim of this article is to provide a systematic framework for microtopographic studies using close-range remote sensing technologies. This is achieved by reviewing the application of close-range remote sensing to capture microtopography and develop microtopographic models in natural ecosystems. Close-range remote sensing techniques such as small Unmanned Aerial Systems (sUAS) and LiDAR technologies have enabled researchers to employ these technologies repeatedly during different seasons to identify the impact of microtopography on the seasonal distribution of vegetation, hydrological connectivity, and GHG fluxes. Small but critical features that are often missed in satellite imagery can be revealed by aerial and terrestrial LiDAR or in sUAS-based photogrammetry in low or sparsely vegetated wetlands.

### *1.4. Research Question*

The main objective of this article is to provide a systematic framework for microtopographic studies using close-range remote sensing technologies. In the past, the characterization of microtopography over large areas was difficult due to limitations in the ability to collect the density of data necessary to represent microtopographic features. The most common methods of measuring microtopography involve extensive manual surveys or transect-based manual surveys and utilizing remote sensing techniques such as aerial surveys and LiDAR-based techniques. To characterize microtopography in a study site, a researcher should focus on answering the following questions: (1) What terrain attributes can represent the microtopography? (2) What spatial resolution of terrain attributes is needed to represent the microtopography? (3) What methodology should be adopted to collect data at the selected resolution? (4) How should microtopography be quantified?

Thus, in this article, to achieve the main objective, we focus our discussion on addressing these four aforementioned questions, to assist researchers in optimizing the use of these new technologies in support of microtopography-based ecosystem studies (see Figure 1).

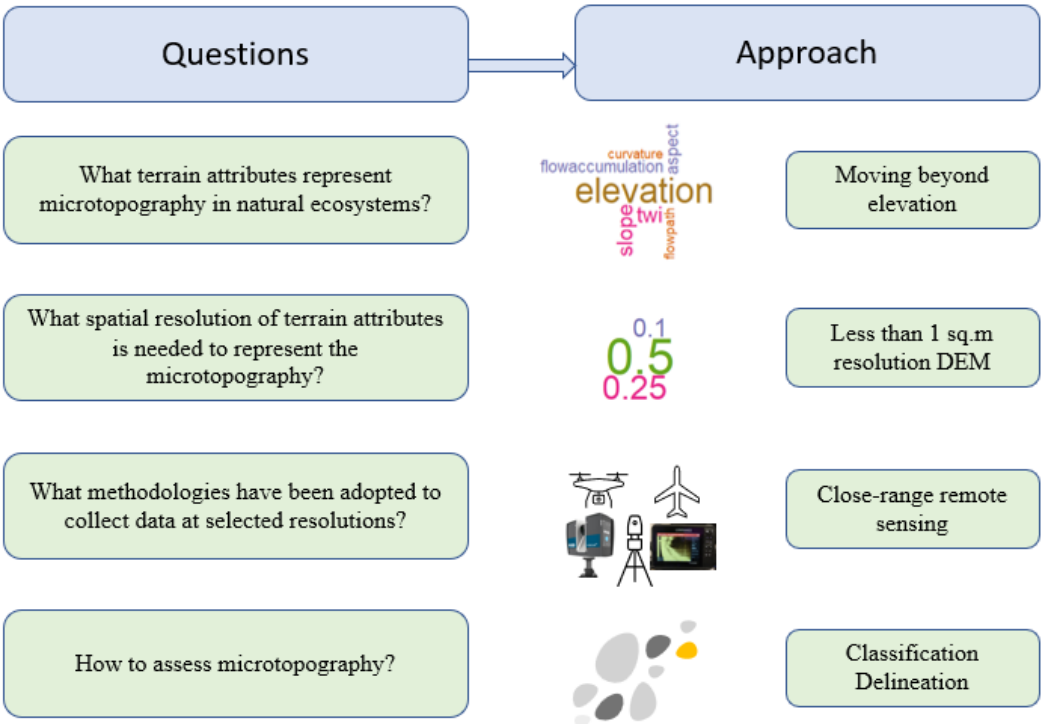



**Figure 1.** Framework to answer microtopography-based questions using close-range remote sensing techniques.

## 2. Terrain Attributes for Representation of Microtopography

Microtopography studies often require the use of quantitative measures to represent microtopographic characteristics. These quantitative measures mainly include terrain attributes (quantified as a continuous spatial variable based on elevation) and landscape metrics (quantified as a categorical spatial variable). Terrain attributes are the quantities that express the position and orientation of ground points [36]. Terrain attributes can be determined using DEMs, which are based on elevation as a continuous spatial variable. Terrain attributes include but are not limited to, elevation, aspect, slope, flow path, flow accumulation, and topographic index. Elevation is the primary attribute for assessing microtopography, but other terrain attributes such as roughness, slope, and terrain indices can also be critical in characterizing microtopography. Table 1 summarizes a variety of ecosystem features impacted by microtopography with corresponding terrain attributes and spatial resolution.

**Table 1.** List of microtopography-based studies with associated terrain attributes and DEM resolution. (RMSE: root mean square error; unit: meters).

| Study Area | Study Objective | Associated Terrain Attribute | Resolution in (m) | DEM RMSE (m) | Characteristics of the Study Site | References |
|---|---|---|---|---|---|---|
| Pennsylvania, USA | Microtopography | Elevation<br>Slope<br>Curvature | 1.00 | 0.18 to 0.37 | Ridge | [37] |
| South Carolina, USA | | Elevation | 0.25 | 0.04 | Tidal forested wetland | This Study |
| Minnesota, USA | | Elevation<br>Slope<br>Roughness<br>TRI | 0.01 to 2 | 0.024 to 0.058 | Forested wetland | [25] |
| Minnesota, USA | | Elevation<br>Slope<br>Concavity | 0.10 | 0.04 | Forest | [2] |
| Banff National Park, Canada | | Elevation | 0.05 to 2.00 | 0.052 to 0.082 | Open shrub wetland | [38] |
| Queensland, Australia | Mosquito management | Elevation | 1.00 | 0.042 | Mangrove | [39] |
| Tabernas Desert, Spain | Erosion | Elevation<br>Roughness | 0.01 | - | Hillslope system | [40] |
| South Carolina,USA | | Elevation<br>Flow accumulation<br>Curvature<br>TWI<br>Slope | 1.00 | 0.04 | Gully | [41] |
| East Siberia, Russia | Carbon storage | Elevation | 2.00 | - | Tundra | [42] |
| Northern England | Roughness | Elevation<br>Slope<br>Ruggedness | 0.005 | - | Blanket Paetland | [43] |
| Alaska, USA | GHG Emissions | Elevation | 2.00 | - | Tundra | [44] |
| Minnesota, USA | | Elevation | 0.10 | 0.04 | Forest | [33] |
| Alaska, USA | Hydrological Processes | Elevation | 0.25 | - | Tundra | [45] |
| Alaska, USA | | Elevation | 0.20 | 0.05 | Tundra | [46] |
| Alaska, USA | | Elevation | 0.50 | 0.023 | Tundra | [47] |

**Table 1.** *Cont.*

| Study Area | Study Objective | Associated Terrain Attribute | Resolution in (m) | DEM RMSE (m) | Characteristics of the Study Site | References |
|---|---|---|---|---|---|---|
| Colorado, USA | Species composition Species richness | Elevation Slope Curvature TPI TWI Flow accumulation | 0.50 | 0.15 | Hillslope system | [48] |
| Minnesota, USA | | Elevation | 0.01 | 0.024 | Forested wetland | [32] |
| Mexico | | Elevation | 0.10 | <1.00 | Tidal wetland | [49] |
| Hungary | Vegetation Pattern | Elevation Slope Aspect Curvature TPI TWI | 0.25 | - | Grassland | [50] |
| Sumatra, Indonesia | | Elevation | 1.00 | - | Forest | [51] |
| North Wales, UK | | Elevation Ruggedness TPI TWI | 0.20 | <0.75 | Blanket peatland | [52] |
| Colorado, USA | | Elevation Slope Curvature TPI TWI Aspect | 0.50 | - | Hillslope system | [53] |
| Singapore | | Elevation | 1.00 | - | Mangrove | [54] |
| Alaska, USA | NEE | Elevation | 0.50 | <0.068 | Tundra | [55] |
| Hawai'i, USA | Species recovery | Elevation | 1.00 | - | Arid | [56] |
| New York, USA | Soil Characteristics | Elevation Slope Aspect TWI Flow accumulation | 5.00 | <6.00 | Mountainous landscape | [36] |

**Table 1.** *Cont.*

| Study Area | Study Objective | Associated Terrain Attribute | Resolution in (m) | DEM RMSE (m) | Characteristics of the Study Site | References |
|---|---|---|---|---|---|---|
| Texas, USA | Soil Characteristics | Elevation<br>TWI<br>Flow accumulation | 10.00 | <10.00 | Plains | [57] |
| Alptal, Switzerland | | Elevation<br>Slope<br>Curvature<br>Aspect<br>Ruggedness<br>TWI<br>Flow path<br>Flow accumulation<br>SPI | 0.5 | 0.12 to 0.45 | Mountainous landscape | [26] |
| Suhua Highway, Taiwan | Landslide | Elevation<br>Slope | 1.00 | 0.04 | Coastal Highway | [58] |
| Isfahan, Iran | | Elevation<br>Slope<br>Curvature<br>Aspect | - | - | Hillslope system | [59] |
| Roznow Lake,Poland | | Elevation<br>Slope<br>Aspect<br>Flow direction | 1.00 | - | Lake side | [60] |

- data not available.

Another terrain attribute that has not been widely explored for microtopographic studies of natural landscapes is surface or soil texture [61]. Surface texture can be related to the microforms such as hummocks or hollows and can be related to surface roughness. The roughness values are calculated based on a prescribed window size and estimated for each window to capture the complexity of the terrain. In addition, once microtopography is classified and delineated as hummocks or hollows, these hummocks or hollows are landscape patches that are categorical spatial variables in nature. Thus, landscape metrics [62], originating from the domain of landscape ecology can be used to analyze the spatial characteristics of these microtopography patches with respect to their composition and configuration. More details on landscape metrics will be discussed in Section 5.

## 3. Spatial Scale of Microtopography

The scale of the microtopographic features of interest is an important consideration. Small variations in elevation matter when it comes to representing microtopography and its associated physical, biogeochemical, and ecological processes. In other words, the study of microtopography often operates at small spatial scales, which often requires high spatial resolutions to capture microtopographic features at smaller spatial scales. Spatial resolution refers to the actual ground size that a pixel represents or the smallest possible geospatial feature that can be detected. Spatial resolution needs to be fine enough in order to capture the information of a geospatial feature. Specifically, spatial resolution needs to be finer than the scale that a geospatial phenomenon operates on (i.e., operational scale; see [63,64]. Therefore, a high-resolution DEM is needed to detect small elevation changes (often at sub-meter level) in the microtopography, which operates at a small spatial scale. This fine spatial resolution need is reflected in the literature (see Table 1; ranging from 0.005 m to 10 m; most of them are under 1 m).

It is necessary to identify what spatial resolution of terrain attributes can adequately represent the microtopography at a specific location. With LiDAR data, it is possible to obtain sub-centimeter resolution DEM data, but an important question is what is the right resolution to capture the landscape microtopography? In Baltensweiler et al.'s [65] modeling of soil pH distribution, the most appropriate spatial resolution was found to be 0.5 m with a cross-validated $R^2$ value of 0.62. While Stovall et al. [25] found that a DEM resolution of 0.01 to 1 m was necessary to represent hummocks in a Black Ash wetland system and determined the most accurate classification of 78.7% with a 0.25 m resolution of DEM. The most appropriate resolution depends on what ecological functions one is trying to model and the complexity of the study site itself. Table 1 shows the spatial resolution of DEM used by different studies. High spatial resolution studies can result in microtopographic feature classifications with improved accuracy, which can differ from those obtained from coarser spatial resolutions in the same region. This may lead to different results in the estimation of parameters for models of GHG emissions, hydrologic connectivity, and biogeochemical processes that are associated with microtopography in natural ecosystems. However, the use of high spatial resolutions often leads to data and computational challenges.

The horizontal resolution and vertical accuracy of elevation are significant aspects of microtopographic studies. The DEM resolution can be selected based on the study site and the purpose of the study. Several researchers have examined the effects of DEM resolution in their study sites. Habtezion et al. [66] in their study of the North American prairie Pothole region found that a coarser resolution DEM (>10 m) tended to overestimate ponded areas and underestimate runoff discharge. DEM resolution becomes even more important for low-relief topography where microtopographic features are differentiated by a few centimeters. We used a stochastic depression analysis tool in Whitebox geospatial analysis tools (GAT) [67] to derive depressions from a 1 $m^2$ resolution airborne laser scan (ALS) and a 0.25 $m^2$ resolution terrestrial laser scan (TLS) DEM for a tidal bottomland forest area, as shown in Figure 2. The high-resolution TLS successfully identified the series of hollows at the south end of the study site. In addition, it also provides information on connected and standalone depressions. This means a TLS-based collection methodology more accurately represents this low-relief forested terrain as compared to a coarser 1 $m^2$ resolution ALS DEM, which underestimated the aerial extent of depressions/hollows in this environment.

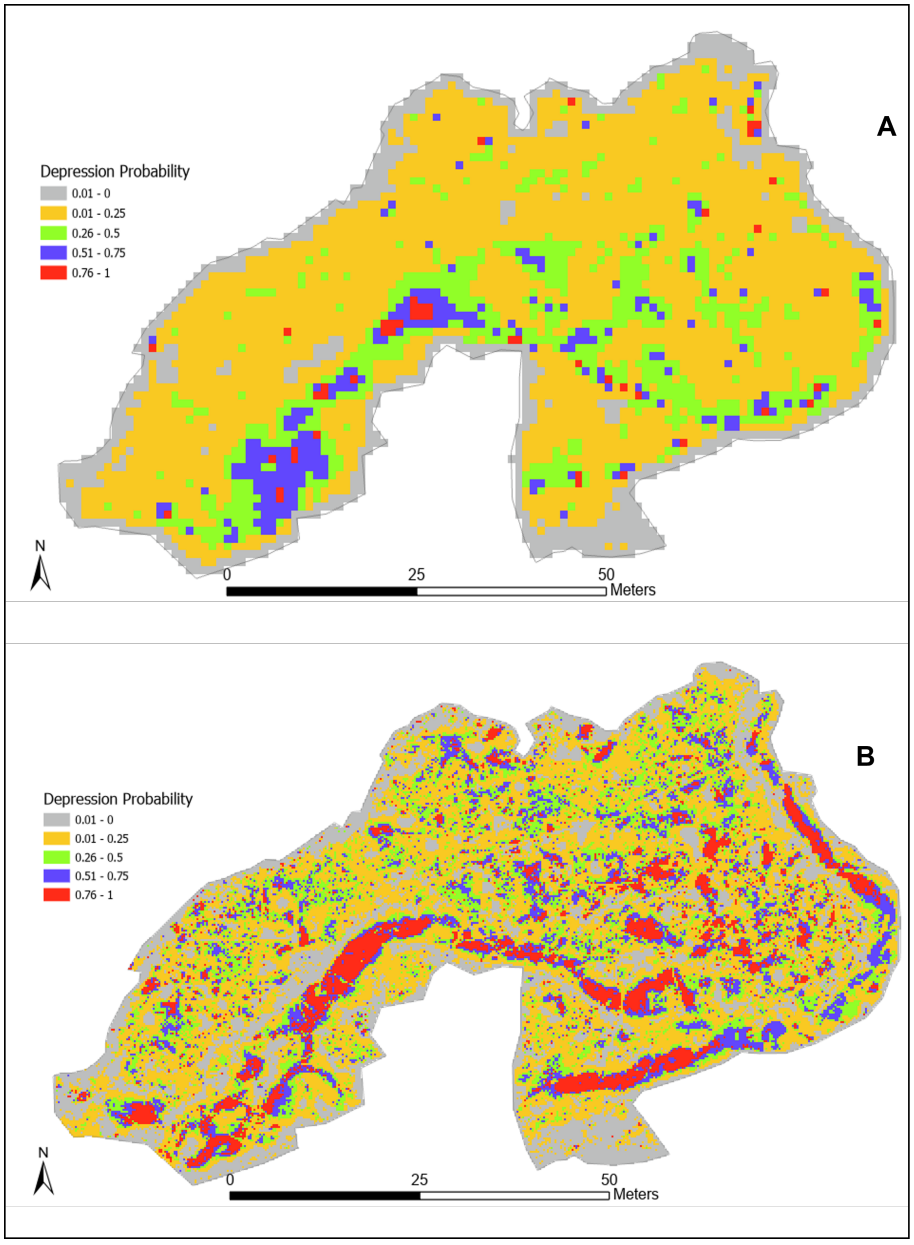



**Figure 2.** Stochastic depression analysis showing the probability of depressions in the Huger Creek forested wetland study site in Santee Experimental Forest, S.C. using (**A**) ALS data and (**B**) TLS data.

## 4. Data Acquisition

Here, we focus on providing guidance as to what remote sensing methodology to adopt to collect data at selected spatial resolutions. Microtopography at high resolutions can only be measured in two ways. First, by extensive manual surveys, and second, by utilizing high-resolution remote sensing techniques. A manual survey requires labor, access to surveying equipment, and the transportation of that equipment to the study site. Most of these studies have used the transects method, using surveying equipment such as total stations, digital levels, or more recently, real-time kinematics global positioning systems (RTK GPS), and they have relied on the categorical analysis of predefined hummocks and hollows [15,68–70]. Transects are often limited in their site representativeness and are relatively ineffective to represent the entire region of interest. In contrast, remote sensing techniques can be used for the purpose of microtopographic mapping of larger areas at a high resolution and affordable cost. For instance, readily available aerial LiDAR data

where point spacing is 1 m or less can provide useful information on microtopography at the field-to-watershed scale.

To decide on the acquisition methodology, researchers need to know the extent of the study area and how much time and relevant resources are available. Based on time and available resources, microtopography can be measured manually or by using remote sensing techniques. Here, we will focus on close-range remote sensing techniques. These methods include aerial surveys with Structure from Motion (SfM) photogrammetry, ALS, and TLS. Combining these measurements with elevations and coordinates obtained with RTK GPS or a total station survey can help georeference the data and validate the remotely collected data. Topographic data collected using more recently developed remote sensing techniques greatly expands the topographic information available as compared to field-level survey approaches employed in earlier studies. Currently, researchers develop a microtopographic model based on the objective of the study and the availability of terrain data. There is no consistent conceptual or analytical framework that provides a guideline to develop microtopographic mapping. Here, we attempt to develop a basic framework involved in estimating the microtopographic features (Figure 3). Here, we discuss each of these methods in terms of the limitations and advantages of these methods (Table 2).

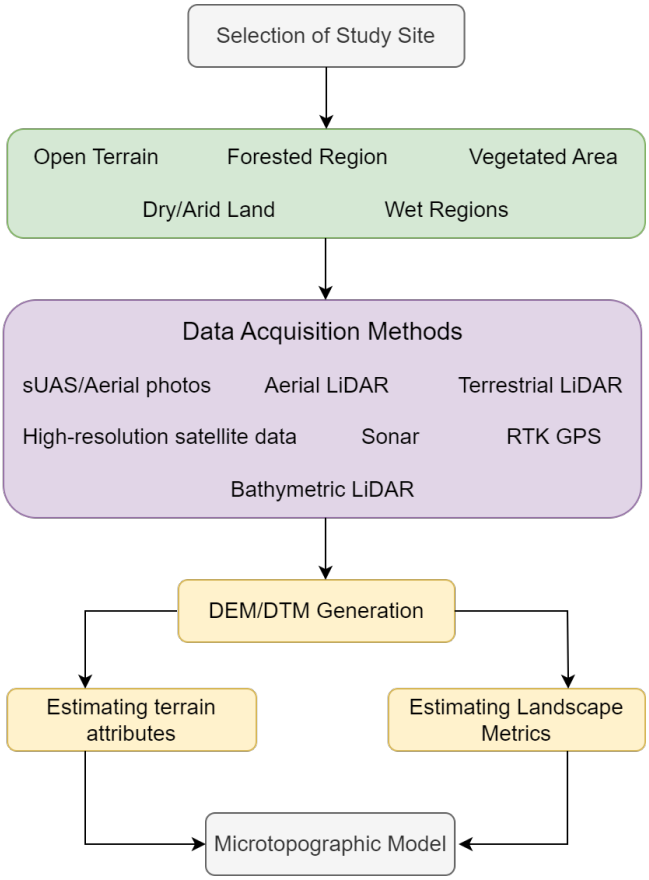



**Figure 3.** Suggested framework for the generation of microtopographic models using close-range remote sensing techniques. The figure shows the data collection method in different terrains, namely, open terrain such as sparsely vegetated terrain, forested areas such as mangroves, vegetated and dry regions such as shrubs and grasslands, vegetated and wet regions such as marsh, and open and wet terrain such as lakes and shorelines.

**Table 2.** Advantages and limitations of close-range remote sensing methods for microtopography data acquisition.

| Data Acquisition Method | Advantages | Limitations | References |
| --- | --- | --- | --- |
| Field Surveys | Data can be used for validation and georeferencing of remote surveys<br>Minimal post-processing of data | Carrying stores and equipment to site<br>Labor Intensive<br>Transect-based studies (5 m to 1550 m transects)<br>Inherent assumption that relatively few observations can represent the whole study site (20–125 observation points) | [25] |
| Aerial photos/sUAS | Cover larger areas compared to field surveys<br>Thermal sensor can detect soil moisture<br>RGB images provide more realistic visualization with high spatial resolution of 0.01 m to 0.05 m.<br>Multiple flight plans can be executed | May require prior permission before flying<br>Post-processing requires technical expertise<br>Flying altitude and velocity impacts data quality<br>Flight duration is restricted by battery life (20 min to 45 min for sUAS) | [71,72] |
| Aerial Lidar | Higher density of laser pulses leads to a higher spatial resolution of 1 $m^2$ or less | Overestimation of ground points in dense forest<br>Horizontal error is in the order of 1/1000 of aircraft flight altitude<br>Post-processing requires technical expertise | [73,74] |
| Terrestrial LiDAR | Can be moved easily to target locations<br>high point cloud density of 20–40 million points per scan<br>Small scan footprint | Low oblique angle data acquisition<br>Post-processing requires technical expertise | [25,72] |

### *4.1. Microtopography Determinations with Field-Level Surveys*

Field-based microtopographic studies generally rely on the use of transects or the study site is divided into multiple sections. The location of transects or subsections is selected based on either topography or species type. Several surveying instruments are used for such surveys including a clinometer, hypsometer, height sticks, level string, dumpy level, and laser range finder. These studies were more common when remote sensing technologies such as LiDAR and UAS were not available. Here, we provide a few examples to show how such surveys were carried out as well as the time and effort that went into those microtopographic studies.

Almquist et al. [75] used a clinometer and two rods at 20 m distances along a transect of 480–1540 m to assess the treefall gaps based on microtopography in a bottomland hardwood forest collecting 24–77 observations. In order to study the diversity of trees and forest structure in tropical freshwater swamp forests in relation to microtopography and water level, Koponen et al. [76] used a hypsometer at 15 m intervals of 10 m $\times$ 50 m sample plots and height sticks to measure the water surface level. The authors considered nine plots to design a transect 530 m long taking 36 observations on the transect. Courtwright and Findlay [12] studied tidal swamps on the Hudson River and found significant porewater and vegetative differences between hummocks and hollows, although the elevation difference was only 19 cm relative to a 1 m tidal range. The authors used a level string that is 20 cm long along a transect to obtain relative elevation. The study considered five transects, each 5 m long with 25 observations on each transect. In another study [77], wooden poles at a certain distance along the transect were used to obtain the elevation and study forest structure in a coastal Mexico lagoon.

All these studies attempted to collect elevation data which now can be easily collected with LiDAR and UAS-based technologies. Along with close-range remote sensing technologies, total stations and RTK GPS are the most widely used field surveying instruments that are being used to validate and georeference remotely collected data.

### *4.2. Microtopography Obtained with Photogrammetry*

sUAS-based SfM photogrammetry is best suited for wetlands where trees are absent or have a low tree or shrub cover [2]. The sUAS-based SfM photogrammetry has been used in various wetland terrains including mapping moss in Antarctica [78], mapping alpine peatlands in Canada [38], quantifying roughness for different peat surfaces [43], and evaluating the impact of seismic lines on peatland $CH_4$ emissions [79]. An sUAS represents a low-cost sensor platform that can cover a wide area, as compared to a tripod or even vehicle-mounted terrestrial LiDAR with several flight missions possible within a few hours. Although the RGB-based camera on a sUAS can provide high-resolution images, in the case of forested wetlands, the data under a forest canopy cannot be captured and, therefore, currently their use is not suitable for microtopographic studies in forested environments. The sUAS with thermal sensors can effectively detect variable soil moisture conditions that can be associated with hummocks/hollows complexes [80]. Near-infrared (NIR) and multispectral cameras can be used to characterize vegetation and analyze the impact of microtopography on vegetation types. The flying altitude and velocity of sUAS also play an important role in the quality of data collection.

#### 4.2.1. SfM based Photogrammetry

In the SfM photogrammetric technique, a mosaic of images is created and then georeferenced using ground control points (GCPs). This technique creates a very high-resolution 3D point cloud which is utilized to create a high-resolution DEM or digital surface model (DSM) as per user requirements. The process has been explained by a number of researchers (e.g., [38,81]). In general, the SfM analysis provides 3D information from stereoscopic 2D images. The process involves the identification of common points called key points. The commonly used algorithm for feature detection is Scale Invariant Feature Transform (SIFT, [82]), which identifies key points in the image. The key points are the unique characteristics of an

image. These key points are invariant of image rotation and scale and remain robust with changes in illumination and the addition of noise. An initial sparse point cloud is created following bundle block adjustment and a high-resolution 3D model is created based on stereoscopic images. The GCPs assist in improving the accuracy of the bundle adjustment and a 3D georeferenced model is generated from a 3D point cloud.

In the case of open topography, RGB camera-based sUAS can assess microtopography effectively. The sUAS-derived SfM photogrammetry can create DSM of sub-centimeter resolution with marked GCPs. Figure 4 shows the DSM of a relatively open topography of a low-relief clear-cut forest in coastal South Carolina, USA. The orthomosaic was developed from the SfM technique using 570 images with 80% side and front overlaps, covering an area of 180,000 sq. meters (using Pix4DMapper software). A total of six GCPs were established using RTK GPS and the images were georeferenced using these GCPs, with a mean root mean square error (rmse)of 0.006 m. Pix4DMapper software was used to develop the orthomosaic.

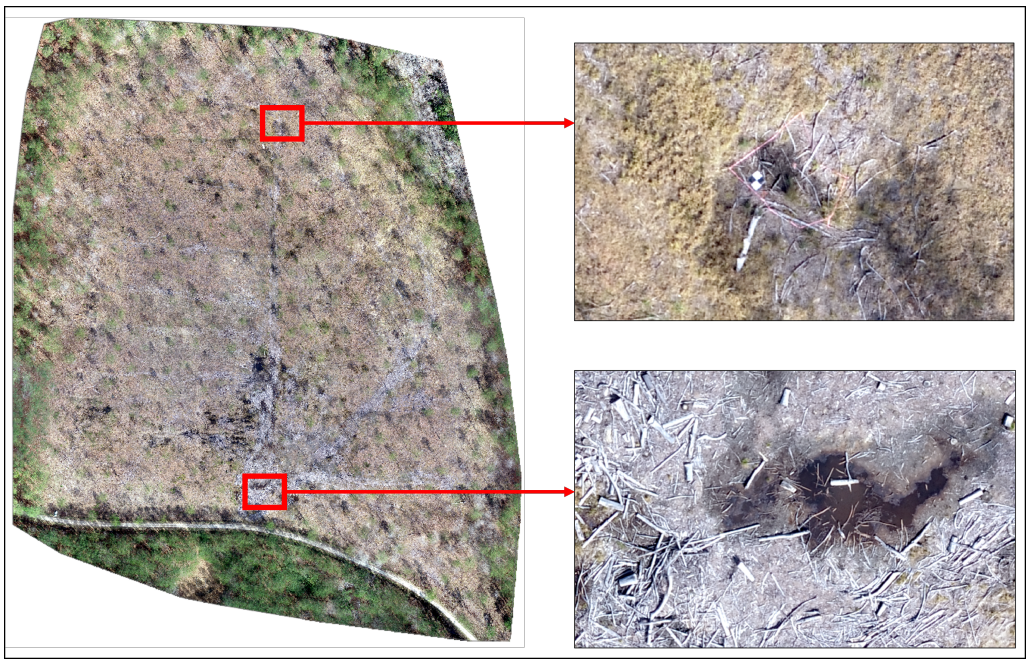


**Figure 4.** The high-resolution DTM of a low-relief coastal forest (2 cm spatial resolution) orthomosaic developed from SfM photogrammetry method using 570 images.

#### 4.2.2. Topographic Models for Microtopography

Quantifying microtopography with aerial photos is inherently related to the purpose of a study. Harris and Baird [52] used a fine-scale topographic model to evaluate the drivers affecting vegetation patterning. Their study found mean elevation as the most influential variable in blanket peatland vegetation patterns due to the high correlation of vegetation with topography and soil moisture. Martinez Prentice et al. [61] used a high-resolution microtopographic model of six wetlands in Estonia using sUAS to analyze the distribution of plant communities. The elevation difference of these wetlands varied between 0 and 3 m and both object- and pattern-based classifications were performed to analyze the distribution of grasslands.

Although sUAS-based photogrammetry techniques can provide high-resolution low-cost 3D topography, this technique has limited applications in dense forest environments. In the case of forested wetlands, sUAS are generally used for the estimation of aboveground biomass density, leaf area index, and vegetation pattern for delineating a wetland boundary. A few studies have also utilized sUAS-based photogrammetry for the estimation of GHG fluxes. Becker et al. [83] utilized a dirigible type sUAS for image acquisition and concluded that the spatial resolution of a DEM impacts the detection of biogeochemical hot spots

with respect to $CH_4$ and $CO_2$. Lehmann et al. [84] used infrared images captured by sUAS to estimate uncertainty in $CH_4$ flux in a South Patagonian peatland related to site microtopography. They considered the distribution of vegetation and microform to estimate the $CH_4$ emission at an ecosystem scale.

sUAS-based measurements of microtopography can cover reasonably large spatial extent of up to few square kilometers, which is a major advantage over conventional transect-based analysis or manual field survey approaches. It provides an affordable solution to quantify the microtopography at a fine spatial scale. The ease of operation enables researchers to collect data multiple times and conduct the analysis of spatial variations over time. These operations must be carefully planned based on considerations of available battery life. Adverse weather conditions need to be avoided to ensure the safety of equipment, and the quality of data, as well as to comply with legal requirements. Quantifying wetland microtopography in forested wetlands and upland forests is more problematic due to the presence of an often dense upperstory and understory. In these environments, large errors in measurement can lead to unreliable or low accuracy of the resultant microtopography mapping. In contrast, open topography such as bogs, boreal wetlands, and peatlands with sparse vegetation can be assessed for microtopography at high spatial resolutions. Currently, the two most popular photogrammetric software used by researchers are Agisoft Metashape and Pix4DMapper [85]. Both are proprietary software, which can provide cloud-based processing and utilize a large collection of images without the need for system upgrades on the user side. Alternative options include open-source software such as OpenDroneMap, openMVG, VisualSFM, and MicMac, which are also available but require technical expertise from users.

### *4.3. Microtopography Acquisition with Aerial LiDAR*

Aerial LiDAR has been used to assess forest canopy structure, underlying terrain, and sub-canopy vegetative structure. In aerial LiDAR scanning, the laser pulses are emitted from the airborne platform and then the backscattered signal from the sensor to the earth's surface is measured, which provides the range estimation between the LiDAR device and the earth's surface. This process is explained in detail in [86]. Chasmer et al. [87] called the frequency distribution of the returns from LiDAR scans a "digital fingerprint" for the natural environment with an assumption that different parts of wetlands and forests have different vegetation structures and morphological characteristics. Aerial LiDAR housed on fixed-wing and sUAS platforms has also been used extensively for estimating surface roughness [37] and mapping forested wetlands [88]. The LiDAR-based sUAS are comparatively more costly than camera-based sUAS but they can effectively capture spatial variations or hummocks/hollows complexes in a vegetated study site depending on the bare ground point density.

The high pulse density and/or small scan footprint associated with LiDAR systems are an asset in mapping microtopography. The LiDAR echoes are processed to create a digital terrain model (DTM). In aerial LiDAR, the higher the pulse propagation frequency the greater the pulse return density per unit area is. A higher density of pulses leads to a higher spatial resolution that can be utilized to construct a high-resolution DTM. To create the representation of a site's microtopography, researchers use ground returns with pulse density of 2 pts/square meter or higher and create a DEM of 1 m or higher spatial resolution (grid cell size of 1 m or less). The cells that do not contain a return are filled with interpolation techniques such as the nearest neighbor, spline methods, inverse distance weighted (IDW), Kriging, and triangulated irregular network (TIN) interpolations [89].

### *4.4. Microtopography Acquisition with Terrestrial LiDAR*

In measuring landscape microtopography the scanner in a terrestrial LiDAR system is mounted on a tripod and can be moved easily to target locations. The laser intensity is inversely proportional to the square of the distance/range while in ALS atmospheric

condition also plays a significant role. In contrast to ALS, the incidence angle impacts the data quality of TLS. The number of scans varies as per study site, terrain, and research question. Terrestrial LiDAR data collection is prone to shadowing effects and occlusion. This can be overcome by scanning the study plot from multiple angles and overlapping scan locations. The registration of multiple scans requires tie points, which are common points used to align and register the point cloud. Artificial objects such as cylindrical reflectors or spherical targets or checkered markers are placed in each location to be scanned and are later used as the tie-points. More scans are required for fine-scale terrain modeling to capture the impact of microtopography on, for example, ecosystem functions. As the point density decreases linearly with distance, the LiDAR data acquisition should, therefore, be planned beforehand to consider the terrain.

The terrestrial scanners generate higher point cloud density compared to the aerial LiDAR. However, aerial LiDAR covers a larger area as it acquires data at near nadir view angles while TLS, due to its low oblique angle of transmitting signals, covers substantially smaller areas. The dense vegetation in forests creates occlusion and shadowing as the signals get interrupted or reflected on their way to the scanner. As the scan distance increases, the probability of returned signal originating from a non-ground object also increases. This leads to an overestimation of ground elevation. This is the reason why there is an overestimation of ground elevation exhibited by both terrestrial and aerial LiDAR in dense forests. For complex study sites, TLS data are more favorable as compared to aerial LiDAR [65]. The main limitation of TLS-based surveys is that they are required to move to multiple scan positions to ensure overlapping scans and to cover the study site. The point cloud density is higher around the scanner and inversely proportional to the square of the distance to the TLS position [90]. In addition, due to the shadowing effect in forests, it becomes more difficult to separate ground surface and non-ground points [91]. To overcome this limitation, a larger number of scans with different viewsheds is required.

The use of terrestrial LiDAR for capturing bare ground in a vegetated region is more challenging. Data acquisition should be planned during the dormant season when leaves are off, and grass and bushes are largely senesced. This will help in addressing the issue of occlusion due to a dense understory. The original point cloud data collected from LiDAR cover both ground and surface returns such as trees and shrubs, which requires cleaning through the use of stray/noise filters to remove spurious or noisy scan points and above-surface scan points. This process may require a number of iterations until most statistical outliers are removed. The resultant filtered point cloud can then be used for further analysis or delineation of hummocks and hollows. The registered and filtered point cloud collected from terrestrial LiDAR is used for subsequent analysis. To analyze the microtopography, the point clouds associated with the ground are retained, which means that point clouds above the ground are required to be removed.

The ground points can be extracted from the dense point cloud generated by terrestrial LiDAR to create a high-resolution DEM. Several researchers [2,25,27,32,92,93] used open-source CloudCompare software to extract ground points. The extraction of ground points requires a point cloud library (PCL, see [94]) to remove noise and outlier points. PCL assumes a normal distribution of points where outliers can be removed based on a defined threshold value of standard deviation. The resultant point cloud can be rasterized for subsequent analysis. Another useful tool that can be used to extract ground points is the use of a cloth simulation filter (CSF) [95]. This method imagines a piece of cloth over the point cloud which is turned upside down. In other words, an imaginary cloth is assumed over an inverted surface, which can classify points as ground and non-ground points, as shown in Figure 5.

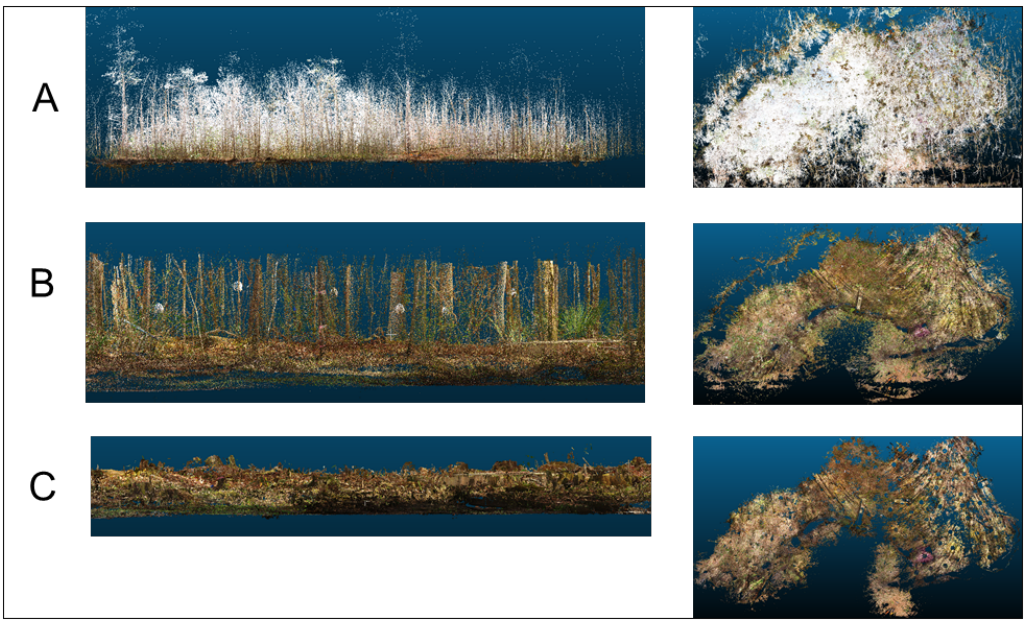



**Figure 5.** Side- and top-view of the TLS point cloud data obtained in a bottomland forested wetland site. (**A**) Raw TLS data are filtered and exported, (**B**) Point cloud clipped to 1 m, (**C**) 1 cm Surface Model.

Here, are a few guidelines for conducting the terrestrial LiDAR-based survey: (1) conducting reconnaissance of the study site before carrying out actual surveying. This will assist in deciding the minimum distance between the scan positions. The location of GCPs can also be decided during this time. (2) Establishing GCPs or fixed spherical targets and measuring them with RTK GPS. (3) The scan positions can be decided based on transects where each transect is separated by 10 m and each scan position is separated by 10 m in a forested landscape. In other landscapes, this distance can be increased depending on occlusions. In a dense forest with understory and shrubs, the scanner can be set at a high point cloud density of 20–40 million points. This will assist in the automated registration of multiple overlapping scans. (4) The control targets or tie points should be evenly distributed with a minimum of 3–5 spherical targets that should be common in adjacent scans. In forested ecosystems, the spherical targets should be increased from 5 to 8. (5) Before processing the point cloud, the minimum distance between the points can be kept at 1 cm. This will greatly reduce the number of points, the resultant point cloud can be used for further assessment and analysis.

## 5. Assessing Microtopography

Assessment of microtopography typically consists of two steps: delineation of microtopographic features and evaluation of delineated microtopographic features. In this section, we focus our discussion on these two steps for the assessment of microtopography.

### *5.1. Delineation of Microtopographic Features*

Delineation of microtopographic features mainly includes three approaches: (1) threshold-based classification, (2) mechanistically based delineation, and (3) machine learning-based delineation.

#### 5.1.1. Threshold-Based Classification of Microtopographic Features

The common way of extracting microtopographic information from field-based surveys is to use transects or plots in the study site and classify microtopographic features, such as hummocks and hollows based on the field experience or sparse measurements. With the availability of close-range remote sensing techniques, the microtopographic features can be delineated over a larger area based on different criteria. Graham et al. [2]

identified three ways to characterize microtopography: (1) based on drivers associated with an ecological function such as using water table depth, (2) elevation distribution of the study plot and classifying hummocks and hollows based on a threshold, and (3) classifying microtopography based on an index, specifically "hollow index", which is calculated using elevation, concavity, and slope.

Multiple researchers used elevation-based thresholds to categorize hollows and hummocks from a DEM generated from sUAS or LiDAR data. The threshold elevation is determined based on field characteristics, expert knowledge, and assumptions. Kalacska et al. [96] conducted a study on three tidal marshes in Canada using sUAS and aerial LiDAR and found the accuracy is comparable to RTK GPS with $R^2$ values of 0.99 and 0.83 for the two methods, respectively. In their study, the authors used expert knowledge to define the height range of 5–31 cm above the median elevation to define hummocks while >5 cm below the median height range were characterized as hollows. Knight et al. [39] analyzed microtopography along a transect in mangroves in Queensland, Australia. They used a 1 m resolution DEM from LiDAR data and generated contours at an interval of 0.05 m. Then, the microtopography was analyzed along a transect where hummocks were identified as positive deviations that are >0.05 m above the local mean elevation and hollows as deviations that are <0.05 m below the mean elevation.

The categorization of microtopographic features is also guided by the aim of the study. Kelly et al. [80] differentiated hummocks and hollows based on vegetation types. The sites with *Sphagnum* sp. were classified as hollows while vascular vegetation sites were classified as hummocks. Griffin et al. [97] generated a LiDAR-derived DEM to analyze the impact of microtopography on mosquito habitats. Brubaker et al. [37] used a pit-filled DEM and then subtracted it from the original LiDAR-derived DEM to identify pit and mound topography within an oak/hickory forest in Pennsylvania, USA.

In addition to elevation, the slope has also been used extensively to categorize microtopographic features. Alexander et al. [51] generated a DTM derived from LiDAR-based data and calculated slope within a 10 m radius of each tree and then analyzed the impact of slope on tree height in a tropical forest in Sumatra. Moreover, the information on the intensity of LiDAR can also be used for the validation of classified features. Korpela et al. [98] used aerial LiDAR in a boreal bog in southern Finland to assess microtopography and analyzed the intensity of echoes that was the highest in hummocks and lowest in water and hollows. That study employed a grid size of 20 cm × 20 cm, hummock index, and depression index to measure the elevation with respect to local water level along with the echo intensity to classify microtopography. A coefficient of +1 or −1 was assigned based on high or low elevation respectively. A value of +8 indicated a perfect peak while −8 corresponded to a depression. The LiDAR returns were analyzed concurrently with aerial imagery in red, green, and blue bands to classify different microtopographic features. The LiDAR/photogrammetry combination worked well in this open bog region as there was nominal occlusion by trees. This also shows that shortwave infrared LiDAR intensity varied with the microtopographic features and is a good indicator/predictor of the spatial distribution of hummocks, hollows, and lawns.

Anderson et al. [99] collected the data over a transect of 10 m at seven different sites, and the vegetation pattern was analyzed in the quadrats of 20 cm × 20 cm. RTK GPS was used to measure elevation along the transect at 50 cm intervals. The hollows and hummocks were identified based on the water level readings and RTK GPS readings. Baltensweiler et al. [65] derived a high-resolution DEM at different scales of 0.2 m, 0.5 m, 1.2 m, and 4 m to create a soil pH model and found 0.5 m model predicted the soil pH most accurately but [65] used a priori information to stratify the study area in depression and ridges. Zhang et al. [100] classified their coastal forested study region into tall and short vegetation and bare ground object.

5.1.2. Mechanistically-Based Delineation of Microtopographic Features

The DEM developed from close-range remote sensing techniques is highly precise and captures microtopographic features, which are natural depressions and not spurious depressions. While delineating depressions such natural depressions should be preserved over artifacts. To identify natural depressions, [101] proposed to combine the "DEM-unchanged" (original DEM) strategy and the "DEM-revising" (filled DEM) strategy based on the study area and data characteristics. Recently, [102] proposed a level-set method that is based on graph theory to delineate nested depressions and a priority-flood algorithm [103] to identify depressions. In a low-relief complex topography, these methods can be useful as they can delineate nested depressions (Figure 6) and can provide insights into the hydrological connectivity of depressions.

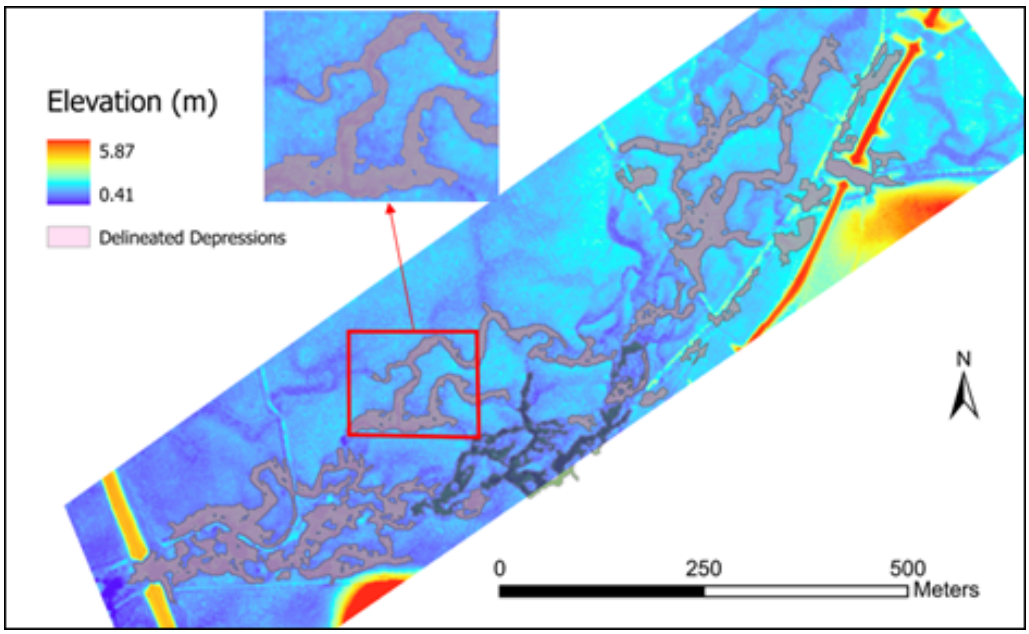



**Figure 6.** Depression delineation using a priority-flood algorithm and level-set method based on aerial LiDAR-derived DEM of 1 $m^2$ resolution in a low relief tidal wetland at Huger Creek area in Santee Experimental Forest South Carolina. The depressions are delineated based on the size of a minimum 1 $m^2$ area and minimum depth from the water surface to the spill point as 0.50 m.

Another method of delineating hollows is utilizing a localized contour tree approach to identify individual hollows. Wu and Lane [104,105] delineated wetland hollows in the prairie pothole region of North America and represented them in the form of contours. A power function curve fitted to the storage area-to-volume relationship provided an area-to-volume model for estimating the storage volume of wetland hollows in the watershed. Most of the hollows in the DEM represented areas that are either inundated continuously or inundated seasonally. Chu et al. [106] proposed a puddle-to-puddle (P2P) modeling framework based on identifying depressions and their hierarchical relationships. The method simulates the surface inundation by filling, spilling, and merging the cells based on the hydrological connectivity and finally delineating the depressions. To delineate hummocks [25] used the watershed delineation approach by inverting the elevation values in the surface model and finding edges of the watershed that actually represents hummock edges. The delineated microtopographic features then can be analyzed for physical characteristics such as area, volume, and depth/height.

5.1.3. Machine Learning-Based Delineation of Microtopographic Features

A variety of machine learning algorithms have been used for image processing operations. This machine-learning approach can be applied to the extraction of microtopographic

features. Moreover, microtopographic field data can be combined with high-resolution DEM/DSM derived from high-resolution satellite images or LiDAR data. Falco et al. [48] investigated the covariability of field soil resistivity tomography data, vegetation data, and terrain attributes utilizing aerial LiDAR-based DEM and Worldview-2 high-resolution RGB satellite images. Abolt et al. [107] and Witharana et al. [108] used convolution neural networks (CNN), a deep learning approach [109], to extract polygons of various sizes and geometry from aerial LiDAR-based DEM of tundra landscape. Another popular machine learning technique is Random Forest which is based on the use of decision trees and ensemble learning for classification and regression. Multiple researchers have shown that microtopography impacts the location and extent of the plant communities [50,61]. Huang et al. [110] mapped thermokarst landforms automatically using the DeepLab algorithm (based on CNN) using high-resolution SfM-based images over a large area of 6 km $^2$. In addition to delineation, machine learning approaches are also used for sensitivity analysis of microtopography classification [25].

Threshold-based classification only considers the elevation-based threshold, which makes it easy to categorize microtopographic features. The threshold can be determined based on field observation and elevation data/DEM, which can provide a more accurate delineation of the features. Mechanistically-based algorithms not only consider elevation but also slope, flow path, and flow direction of each grid cell. The accuracy of this delineation is highly dependent on the DEM grid size and accuracy as the terrain attributes are derived from DEM. These results should further be validated by sUAS orthomosaics or high-resolution satellite images or field data. Machine learning is best for the automated delineation of microtopographic features over a large area. Other than terrain attributes, we can also include other characteristics of terrain such as vegetation type to delineate the microtopographic features. Although preparing a training data set can be time consuming, it can provide useful information over a watershed scale once the machine learning algorithms are trained.

### *5.2. Evaluation of Microtopographic Features*

The physical characteristics of microtopographic features such as surface area, volume, and depth of hollows, also referred to as morphometric data can be derived from LiDAR data and calculated using several methods. Stovall et al. [25] quantified fine-scale microtopography and delineated hummocks estimating the height, area, volume, and perimeter of individual hummock features. Both Stovall et al. [25] and Lovitt et al. [79] used a moving window average as an elevation threshold to classify microtopography. Brooks and Hayashi [111] used morphometric data and maximum depth (dmax) to measure vernal pools' maximum volume (Vmax), maximum area (Amax), and a p-coefficient to represent the shape of the basin, as shown in Equation (1).

$$V_{max} = (A_{max} d_{max}) / (1 + 2/p) \quad (1)$$

where $p < 1$ represents a convex basin and $p > 1$ corresponds to a concave basin.

A similar approach was used by Gamble and Mitsch [112] for the calculation of wetland area (Amax), depth (dmax), and volume (Vmax) for depressional wetlands, as shown in Equation (2).

$$V_{max} = (0.3219 A_{max} d_{max}) \quad (2)$$

The morphometric data for Figure 6 are shown in Figure 7.

Once microtopographic features are classified and delineated, these features (e.g., hollows or hummocks) are spatial categorical variables that can be further analyzed with landscape metrics [62]. Landscape metrics include, but are not limited to, connectivity, microtopographic features' shape, size, area, perimeter, diversity, and fragmentation (microtopographic features are represented as landscape patches–spatial categorical variables). These metrics can provide important insights into the microtopography studies, which can assist researchers to assess its impact on ecological, hydrological, and biogeochemical

processes in terms of the composition and configuration of microtopographic patches. Here, we show an example of a low-relief wetland area which is categorized based on elevation and water level and analyzed the landscape metrics for the microtopographic features. Figure 8 shows the tidal wetland landscape classified into microtopographic features hollows, hollow fringe, and hummocks using elevation threshold. The data were collected using terrestrial LiDAR. This method clearly delineated the tidal channel present in the study area. This channel gets inundated during high tides but remains exposed to air during the low tides. The corresponding landscape metrics are shown in Table 3.

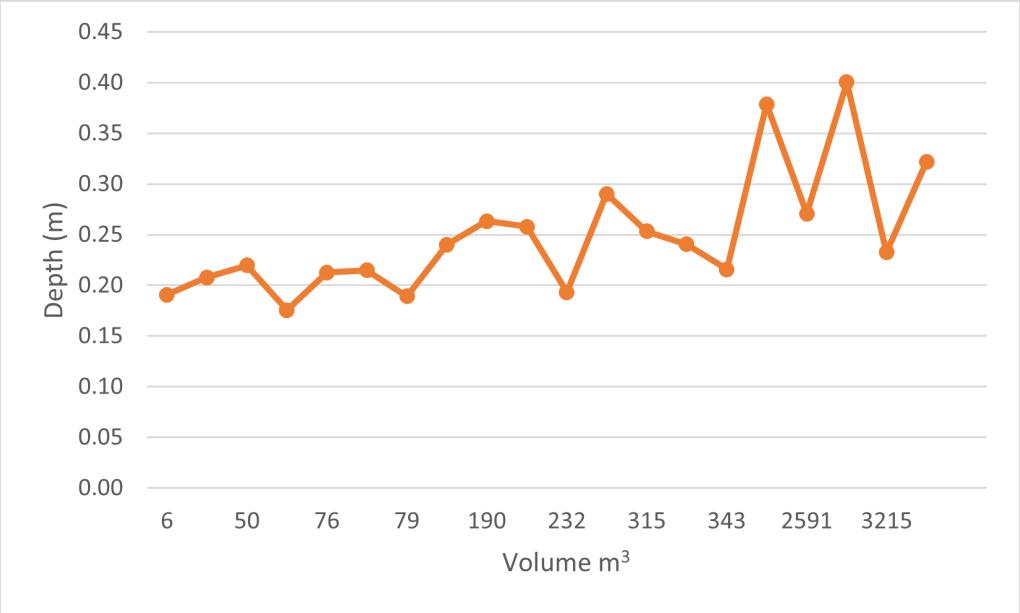



**Figure 7.** The graph shows the morphometric data of the delineated hollows shown in Figure 6—volume in cubic meters and depth in meters for each of the delineated hollows.

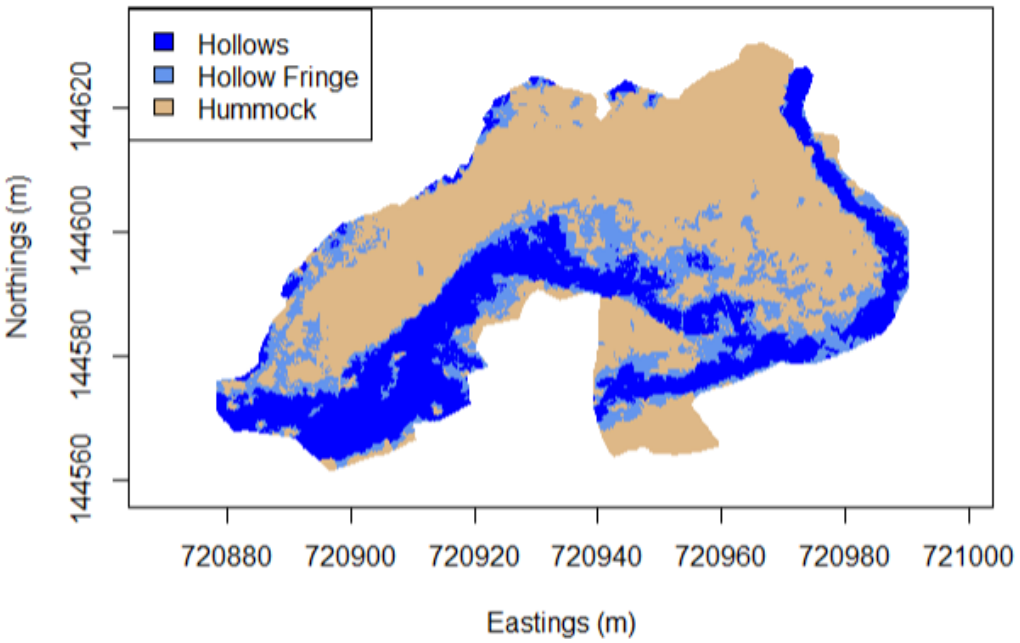



**Figure 8.** Landscape categorization based on elevation threshold: microtopographic features-hollows (<0.65 m), hollows fringe (0.65 to 0.80 m) and hummocks (>0.80 m) based on terrestrial LiDAR DEM with grid cell size 0.25 m × 0.25 m in a low relief tidal wetland at Huger Creek area in Santee Experimental Forest, South Carolina.

There are more than 50 landscape metrics that have been reported so far in the literature [113]. These metrics are designed at patch (e.g., individual hollow patches), class (e.g., hollow or non-hollow), or landscape levels and can be used to quantify spatial features of microtopographic patches at different levels. For instance, the Aggregation index describes how different microtopographic features are spatially associated with one another. The clumpiness index indicates how microtopographic features are aggregated or dispersed. The higher value indicates a more clumped distribution of features while lower values show dispersed distribution. The contiguity index provides information on how microtopographic features are connected. The tidal channel at the study site was characterized by a higher contiguity index compared to hollow fringe and hummocks. Perimeter to area ratio indicates the shape complexity of the features and sensitivity to the feature size. The above indices show that the microtopographic features are more aggregated and clumped in the tidal bottomland forest (Figure 8 and Table 3).

**Table 3.** Landscape metrics (mean values) calculated for a tidal bottomland forest (Figure 8) [113].

| Landscape Metrics | Hollows | Hollow Fringe | Hummocks |
|---|---|---|---|
| Aggregation Index | 0.93 | 0.75 | 0.95 |
| Clumpiness Index | 0.91 | 0.70 | 0.90 |
| Contiguity Index | 0.42 | 0.26 | 0.22 |
| Mean perimeter area ratio | 8.62 | 11.37 | 12.01 |
| Percentage of landscape | 25.27 | 17.90 | 56.53 |
| Mean shape index | 1.25 | 0.97 | 0.65 |

### *5.3. Accuracy Assessment*

The classification of microtopographic features can be validated by producer accuracy (PU), user accuracy (UA), and overall accuracy (OA), which have been well studied in the literature of remote sensing [114]. The computation of Kappa estimates is another popular approach to validate the results. The overall accuracy is usually expressed in percent by taking a summation of correctly classified values and dividing by the total number of values. Producer accuracy, as the name suggests is from the viewpoint of a map producer, it is the calculated number of correctly classified values in a class divided by the total number of values in that class (column total). User accuracy is calculated as the total number of correct classifications for a particular class divided by the row total. The Kappa coefficient ranges from −1 to +1 where a negative value indicates classification is significantly worse than random (by chance) and a value close to 1 shows that classification is significantly better than random. When conducting a study at multiple DEM resolutions it is worth reporting results of multiple accuracy metrics (instead of single metric) for performed classifications as each metric has its own power (see [115]).

## 6. Discussion

Small elevation changes in the natural ecosystems can have a significant effect on ecosystem processes such as biogeochemical reactions. The spatial heterogeneity of different processes requires analysis of microtopography, spatially and temporally at an appropriate scale. For instance, we often observe a wide range of GHG emissions measured within a type of ecosystem, for example, coastal wetlands [116]. One of the possible reasons for these variations is a strong association of GHG emissions with wetland microtopography, which is not incorporated in most biogeochemical models. As suggested by Shi et al. [117], modification of the existing models by incorporating microtopography to assess C exchange results in improved prediction of C emissions.

To represent the microtopography of any study region requires the collection of a huge amount of data which enables researchers to delineate microtopographic features of interest such as hummocks, mounds, and hollows or pits for further analysis. The collection of data can be challenging particularly in forested areas due to their vegetation coverage that is often dense. The vegetation obscures the ground and, therefore, the data collection process

should be well planned. It may require multiple flights or scans to cover a relatively small study area. sUAS and LiDAR-based technology is most suitable in forested wetlands for microtopographic studies while these technologies along with traditional aerial LiDAR and high-resolution satellite images can also be used in areas with limited vegetative cover.

In forested or vegetated regions LiDAR-based data acquisition is most suitable. For microtopographic studies, data should be collected when vegetation is senesced to ensure minimum occlusion. The LiDAR scanner should be set at high point cloud density (approximately 10 to 20 million pulses per scan) and data acquisition should be carried out with multiple overlaps with scan distance not more than 15 m. With aerial LiDAR data the point density is impacted by the flight altitude and speed of the aircraft. LiDAR based on sUAS are most suitable for forested regions as the flight operation can be conducted at a lower altitude and speed can be controlled as low as 5 m/s.

As of now, microtopography is only analyzed or studied as a static spatial phenomenon. It is our understanding that microtopographic features should be analyzed temporally as the spatial heterogeneity varies not only with location but also along the temporal dimension. The ecological, hydrological, or biogeochemical processes exert an impact on the microtopography by erosion or deposition. The temporal element can highlight the impact of such processes on microtopography and vice versa. This can provide useful insights into wetland and forest management. For example, it will also be interesting to see the spatiotemporal impact of saltwater intrusion on microtopography. Our current use of microtopographic representation is mainly limited to the creation of a single static DEM. It has an implicit assumption that microtopography is static and not changing but we need to ask if is that true. This becomes a more relevant question when we say microtopography is not only influenced by elevation but also by other terrain attributes. We also need to investigate how to present and integrate the temporal information of terrain attributes into the microtopographic models if we are to adequately investigate dynamics in microtopography.

Another issue involved with the use of high-resolution microtopographic data is the registration of scans or image alignment in forested environments. The absence of artificial objects makes it challenging to stitch together a large number of scans or images. More spherical targets and GCPs are needed in the case of terrestrial LiDAR scans and sUAS image data collection to ensure successful registration/alignment. Although data can be collected most times of the year in open wetlands, limited time is available for the data collection in forested or vegetated areas and data collection must be planned during the dormant season to reduce the occlusion from vegetation. Direct georeferencing methods can be useful in mapping as they do not require establishing GCPs. Padro et al. [118] compared different direct georeferencing methods and an indirect georeferencing method and found onboard raw GNSS yielded a positional accuracy in excess of one meter with a vertical accuracy in the range of 4 m or higher. However, the post-processed kinematic (PPK) single-frequency carrier-phase without in situ ground support and with ground support were of decimetric and centimetric accuracies. The results were improved further with GCP yielding centimetric accuracy. This shows that other than the GPS method of georeferencing, PPK-based direct georeferencing method can be utilized for forest and wetland microtopographic studies. In this method, the nearest pseudo reference station (PRS) receives differential corrections which further corrects the onboard GNSS position.

### *6.1. Microtopography with Data Fusion*

Data fusion of different data outputs can provide more insights into natural ecosystems as it combines the information from several sensor sources and can provide a more holistic view of a study system. The methodology of data fusion approaches to delineate high-resolution topography can provide direction to adopt ideal ways to represent surface microtopography. Data fusion is not restricted to merging information from different platforms and sensors but also different spatial and temporal scale matching. A reference frame can be defined to which data from different sources and time periods can be trans-

formed. In the future, we propose remote sensing-based microtopography studies which consist of multi-source data integration in the natural ecosystem modeling and an explicit examination of the impact of scale. The collection of field data with explicit topographic information can be used for calibration and validation of the datasets. In addition, data fusion techniques which require combining two or more sensor output data can be useful in analyzing microtopography. There are studies that utilized data fusion techniques which include point cloud data of terrestrial LiDAR and sonar data to map the geomorphology and topography of the hydraulic structures to the study of scours [72]. These studies can be extended to the field of microtopography mapping to generate a more holistic view of wetland and forest systems.

High-resolution satellite data are a relatively new data source for microtopographic studies. Beginning with study areas without canopy cover and then progressing towards more forested study regions. The high-resolution satellite images can provide useful tools to assess GHG emissions, or explore biogeochemistry in relation to microtopography in no/sparsely vegetated regions, although this needs more research. Satellite data used in combination with sUAS or LiDAR data can provide useful information with respect to the impact of microtopography on ecosystem parameters. There are multiple low-orbiting small satellites that can capture images at high spatial, temporal, and spectral resolutions. The list of satellites that provide sub-meter resolution panchromatic images today are (1) WorldView-1 (50 cm), WorldView-2 (50 cm), WorldView-3 (30 cm), GeoEye (50 cm), Pleiades-1A (50 cm), Pleiades-1B (50 cm), Pleiades-Neo (30 cm), SuperView-1 (50 cm), KOMPSAT-3 (70 cm), IKONOS (80 cm), SkySat (72 cm to 86 cm panchromatic and 1.00 m multispectral). Also combining these high-resolution satellite images can provide a context to a study region and its importance.

These high-resolution images can assist in precision agriculture applications, forest canopy estimation, and urban planning. These data sources are currently not being used for assessing microtopography in forested regions, likely because the ground is obscured by the overstory and understory vegetation. The synthetic aperture radar (SAR) which uses an active data collection process means that its sensor produces its own energy and can provide high spatial resolution data compared to other satellite data. As of now, SAR is most suitable for topographic mapping due to its high penetration but its applicability to study microtopography in natural ecosystems is still a matter of research. In the last five years, researchers are actively working on developing algorithms to create high-resolution DEM from SAR data. For example, [119] proposed dual-frequency and dual-baseline (DFDB) configuration in airborne SAR interferometry (InSAR) and a baseline calibration algorithm to create a high-resolution DEM in tidal flats. In their proof of concept, the authors claimed a high vertical accuracy in the sub-meter range. Another study, [120] developed a model for measuring topographic changes in tidal flats and relied on minimizing the errors due to height and interferometric phase deviation. In the InSAR methodology, the quality of the interferogram is based on master and slave images, which means high coherence is important to ensure the accuracy in DEM. The study area examined by both studies is without the canopy cover. Nonetheless, satellite data can be combined with close-range remote sensing technologies to provide greater insights over a large aerialextent.

### *6.2. Utilizing Advanced Techniques*

New LiDAR technologies such as Geiger mode, single photon, and FLASH splits the single laser pulse into multiple pulses. This results in a greater number of returns and therefore a denser point cloud with more information. Such systems can penetrate through a dense forest canopy and detect the microtopography in a forested area although the laser penetration or the number of returns from the ground decreases with increasing tree canopy or ground vegetation cover. These LiDAR systems are more sensitive than earlier LiDAR scanners and are able to detect weak return signals. The lighter weight of these technologies also makes them ideal for flying at lower altitudes. In addition, aerial LiDAR

data are regularly spaced and not very prone to shadowing effects in contrast to aerial photogrammetric techniques.

Moreover, the availability of LiDAR sensors in different wavelengths enables us to choose the sensor based on the research question. Researchers [121–123] have conducted studies to identify wavelength appropriate for vegetation/species classification. The typical wavelengths associated with aerial topographic LiDAR are 1064 nm, 1550 nm, and 905 nm, and bathymetric LiDAR are green-532 nm and infrared (1064 or 1550 nm) [124]. Bathymetric LiDAR are composed of green and infrared beams. The green beam can propagate in water and assist us in finding useful information on geomorphology while infrared beams are reflected by the water providing the water surface elevation.

### 6.3. Microtopography with Bathymetry

The technologies used for bathymetric surveys include echosounders, total station/RTK GPS, unmanned surface vessels (USV), UAS, airborne LiDAR Bathymetry (ALB), and Green-wavelength terrestrial laser scanning (GWTLS). Satellite-derived bathymetric data are of medium resolution and may not be appropriate for the microtopographic studies often operating at small spatial scales. The inundated portion of a wetland or lacustrine margins can also be mapped using bathymetric LiDAR or SfM surveys. For example, coastal zone mapping imaging LiDAR (CZMIL) can not only map the above water topography but the green laser can also penetrate water to some depth and produce high-resolution bathymetric data. Shallow water where boats can not be launched or the streams/rivers or regions which are inaccessible to boats with traditional sonar equipment can be surveyed using RTK GPS or total station. Technologies such as CZMIL and GWTLS have been used for nearshore bathymetry under clear atmospheric and water conditions where the water depth is less than 1 m providing high-resolution microtopography [125]. The laser-based bathymetric measurements are corrected by applying refraction correction which requires specification of water surface level and refractive index. The refractive index is 1.335 for green lasers passing from air to clear water. The submerged point clouds are corrected for refraction while the ground points maintain their original coordinates.

Other than LiDAR surveys, echosounders are the conventional surveying technique used for high-resolution microtopography. It is important to control the speed of the surveying vessel to ensure high point density. The echosounders are generally equipped with a GPS system that provides the coordinates of the measuring point. Unlike LiDAR systems, the echosounders are not restricted by the depth of the water and can survey rivers and streams. The microtopography of river bed deformation or in other words, scour or deposition can be measured using echosounders [126].

### 6.4. Acceleration of Microtopographic Data Analytics Using High-Performance Computing

High-resolution microtopographic data collected via close-range remote sensing techniques are often in large volume, i.e., big data [127]. The use of these high-resolution data comes with its own challenges when we manage, process, analyze, and visualize them (e.g., registration and aligning point cloud data, performing different statistical analyses on point cloud data, and processing high-resolution images and mosaics). The processing and analytics of large-volume microtopographic data are often computationally demanding, which can be overcome by using high-performance and parallel computing approaches to leverage cyberinfrastructure-enabled computing resources [128,129].

The processing and analysis of large microtopographic data can be split into smaller computing tasks that can be allocated to multiple computing elements for acceleration. For example, Barnes et al. [130] developed a parallel priority-flood algorithm for depression filling of large DEM data. Large DEM data were decomposed into individual tiles on which depression-filling operations were applied. Barnes [130] tested the parallel depression filling algorithm on a series of DEM datasets and significant speed up was obtained (only 287 min were needed when using 48 CPUs for parallel processing of the SRTM DEM dataset, compared to 223 h for sequential time using 1 CPU). Zheng et al. [129] implemented a

parallel spatial interpolation approach that relies on 2D spatial domain decomposition for the processing of DEM from LiDAR data. As a result, the overall computing time was reduced from over 17 h down to within 1 h by using 18 CPUs. High-performance and parallel computing as a key capability of advanced cyberinfrastructure have a variety of applications, and it has great potential in accelerating microtopographic data processing and analytics.

## 7. Conclusions

In this article, we provide a systematic data-driven framework to guide the study of microtopography using close-range remote sensing. Our framework focuses on four components: terrain attributes, spatial resolution, data acquisition, and assessment of microtopography. Terrain attributes based on elevation (e.g., slope, aspect, curvature, TWI, TPI, flow path, and flow accumulation) dominate the choice of quantitative measures for microtopography. Further, landscape metrics can also be used for quantification once microtopography is classified or delineated as, for example, hummocks or hollows (spatial categorical variable). With respect to spatial resolution, a high-resolution DEM (often at the sub-meter level) is needed to adequately account for microtopographic characteristics as microtopography-driven phenomena often operate at a small spatial scale. On one hand, we need to make sure the spatial resolution to be used is finer than the operational scale of microtopography. On the other hand, the use of very fine spatial resolutions for microtopographic data will lead to a big data challenge due to the high volume of data to be handled.

Alternative close-range remote sensing techniques (sUAS, aerial LiDAR, and terrestrial LiDAR) have their own advantages and limitations in terms of time, labor, and accuracy. It is important to take into account these aspects together with terrain attributes and spatial resolutions for efficacious microtopographic data acquisition. Multiple studies have shown that remote sensing techniques, especially through ALS, TLS, and sUAS can produce high-resolution DEMs and provide fine-scale measurements of microtopography in natural ecosystems [25,26,32,33]. Some studies have used a combination of one or more remote sensing techniques to delineate natural and human features in the environment [72] but multi-platform remote sensing approaches are not yet commonly employed in combination to delineate microtopography, particularly in low relief forested environments. The combination of one or more techniques of aerial LiDAR, terrestrial LiDAR, sUAS, and high-resolution satellite images is the way forward to characterize the microtopography in complex environments including forests, coastal and forested wetlands. Combining remote sensing techniques with field measurements which include but are not limited to water level data, soil moisture, soil pH, trace gas emissions, and RTK GPS data for location accuracy can provide a robust tool for predicting and assessing the ecosystem functions influenced by the microtopography. There is also a need for increasing the availability of microtopographic data through increased sharing of datasets on platforms like OpenTopography and accelerating microtopographic data processing and analytics via cyberinfrastructure-enabled high-performance computing capabilities. New field-scale measurements of biogeochemical and hydrologic processes that are explicitly linked to topographic metadata are required to further realize the potential of these new technologies and algorithms. The higher 3D point cloud density generated from close-range remote sensing leads to greater accuracy of DEM with lower RMSE (e.g., less than 0.5 m). Our review makes it clear that heterogeneity in the topography of the natural ecosystem influences the biogeochemical and hydrologic processes, which should be included in the ecosystem models when microtopography plays an inevitable role. We also emphasize the need to better model microtopographic features to investigate their impact on ecosystem processes by including field-based observations in the models (i.e., model calibration and validation).

The assessment of microtopography typically includes the delineation and evaluation of microtopographic features. There are three delineation approaches: threshold, mechanis-

tically, and machine learning-based. While the first two approaches have been extensively used in the literature of microtopographic studies, machine learning and deep learning algorithms hold great potential in the automated delineation of microtopographic features and application in large study regions. More machine learning-based studies are highly expected in the near foreseeable future as deep learning-driven artificial intelligence has been increasingly driving data-intensive studies such as microtopographic data analytics in this study. To further analyze classified microtopographic features, landscape metrics can be used to assess spatial characteristics and configuration of the features of interest. We also encourage researchers to move beyond measures of simple elevation and incorporate other terrain attributes such as slope, aspect, flow accumulation, TWI, TPI, and flow path to better predict variations in biogeochemical processes and the spatial character of biotic communities.

Overall, the framework discussed in this article may improve our understanding of microtopography by using close-range remote sensing as a quantitative approach. In future studies, we will focus on specific applications or case studies of microtopography-driven geospatial phenomena, which will provide a more detailed exploration and comparison of close-range remote sensing techniques with respect to their capabilities for empowering microtopography studies. Further, we will explore the power of machine learning-based approaches in the analytics of sophisticated microtopographic data (e.g., automated delineation and recognition of microtopographic features) as well as the utility of high-performance computing in accelerating these analytics that is often computationally considerable.

**Author Contributions:** Conceptualization, T.S.; methodology, T.S., C.A., W.T., C.C.T., G.C. and S.C.; investigation, T.S.; resources, T.S., C.A., W.T., C.C.T., G.C. and S.C.; data curation, T.S.; writing—original draft preparation, T.S.; writing—review and editing, T.S., C.A., W.T., G.C., C.C.T. and S.C.; visualization, T.S.; supervision, C.A. All authors have read and agreed to the published version of the manuscript.

**Funding:** This research received no external funding.

**Data Availability Statement:** The terrestrial LiDAR data and sUAS data presented in this study are available on request from the corresponding author. The aerial LiDAR data is publicly available and can be found here: https://cybergis.uncc.edu/santee/, accessed on 10 January 2023.

**Acknowledgments:** We acknowledge the support of USFS in Santee Experimental Forest for providing resources to conduct the field survey. We also acknowledge the support of the Center for Applied Geographic Information Science for providing financial support to carry out field surveys. The authors would also like to acknowledge Tianyang Chen; Navanit Sri Shanmugam for helping in the data collection of terrestrial LiDAR and sUAS.

**Conflicts of Interest:** The authors declare no conflict of interest.

## Abbreviations

The following abbreviations are used in this manuscript:

| | |
|---|---|
| C | Carbon |
| CSF | Cloth Simulation Filter |
| CZMIL | Coastal Zone Mapping Imaging LiDAR |
| DEM | Digital Elevation Model |
| DSM | Digital Surface Model |
| DTM | Digital Terrain Model |
| DFDB | Dual Frequency Dual Baseline |
| FAA | Federal Aviation Administration |
| GCP | Ground Control Points |
| GHG | Greenhouse Gasses |

| | |
|---|---|
| GNSS | Global Navigation Satellite System |
| GSD | Ground Sample Distance |
| HPC | High Performance Computing |
| InSAR | Interferometry Synthetic Aperture Radar |
| LiDAR | Light Detection and Ranging |
| N | Nitrogen |
| NDVI | Normalized Difference Vegetation Index |
| NIR | Near Infrared |
| PPK | Post Processed Kinematic |
| RGB | red Green Blue |
| RTK GPS | Real Time Kinematics Global Positioning Systems |
| SAR | Synthetic Aperture Radar |
| SfM | Structure from Motion |
| SIFT | Scale Invariant Feature Transform |
| sUAS | small Unmanned Aerial Systems |
| TIN | Triangulated Irregular Network |
| TLS | Terrestrial Laser Scanners |
| VLOS | Visual Line of Sight |

## References


1. Bubier, J.L.; Moore, T.R.; Roulet, N.T. Methane emissions from wetlands in the midboreal region of northern Ontario, Canada. *Ecology* **1993**, *74*, 2240–2254. [CrossRef]
2. Graham, J.D.; Glenn, N.F.; Spaete, L.P.; Hanson, P.J. Characterizing Peatland Microtopography Using Gradient and Microform-Based Approaches. *Ecosystems* **2020**, *23*, 1–17. [CrossRef]
3. McClain, M.E.; Boyer, E.W.; Dent, C.L.; Gergel, S.E.; Grimm, N.B.; Groffman, P.M.; Hart, S.C.; Harvey, J.W.; Johnston, C.A.; Mayorga, E.; et al. Biogeochemical Hot Spots and Hot Moments at the Interface of Terrestrial and Aquatic Ecosystems. *Ecosystems* **2003**, *6*, 301–312. [CrossRef]
4. Sullivan, P.F.; Arens, S.J.T.; Chimner, R.A.; Welker, J.M. Temperature and Microtopography Interact to Control Carbon Cycling in a High Arctic Fen. *Ecosystems* **2008**, *11*, 61–76. [CrossRef]
5. Chmura, G.L.; Anisfeld, S.C.; Cahoon, D.R.; Lynch, J.C. Global carbon sequestration in tidal, saline wetland soils. *Glob. Biogeochem. Cycles* **2003**, *17*. [CrossRef]
6. Moore, T.R.; De Young, A.; Bubier, J.L.; Humphreys, E.R.; Lafleur, P.M.; Roulet, N.T. A Multi-Year Record of Methane Flux at the Mer Bleue Bog, Southern Canada. *Ecosystems* **2011**, *14*, 646. [CrossRef]
7. Helbig, M.; Chasmer, L.E.; Kljun, N.; Quinton, W.L.; Treat, C.C.; Sonnentag, O. The positive net radiative greenhouse gas forcing of increasing methane emissions from a thawing boreal forest-wetland landscape. *Glob. Chang. Biol.* **2017**, *23*, 2413–2427. [CrossRef]
8. Whiting, G.J.; Chanton, J.P. Greenhouse carbon balance of wetlands: methane emission versus carbon sequestration. *Tellus B Chem. Phys. Meteorol.* **2001**, *53*, 521–528. [CrossRef]
9. Zhang, Z.; Zimmermann, N.E.; Stenke, A.; Li, X.; Hodson, E.L.; Zhu, G.; Huang, C.; Poulter, B. Emerging role of wetland methane emissions in driving 21st century climate change. *Proc. Natl. Acad. Sci. USA* **2017**, *114*, 9647–9652. [CrossRef] [PubMed]
10. Bullock, A.; Acreman, M. The role of wetlands in the hydrological cycle. *Hydrol. Earth Syst. Sci.* **2003**, *7*, 358–389. [CrossRef]
11. Lane, C.R.; Leibowitz, S.G.; Autrey, B.C.; LeDuc, S.D.; Alexander, L.C. Hydrological, physical, and chemical functions and connectivity of non-floodplain wetlands to downstream waters: A review. *J. Am. Water Resour. Assoc.* **2018**, *54*, 346–371. [CrossRef] [PubMed]
12. Courtwright, J.; Findlay, S.E.G. Effects of Microtopography on Hydrology, Physicochemistry, and Vegetation in a Tidal Swamp of the Hudson River. *Wetlands* **2011**, *31*, 239–249. [CrossRef]
13. Frei, S.; Lischeid, G.; Fleckenstein, J.H. Effects of micro-topography on surface–subsurface exchange and runoff generation in a virtual riparian wetland—A modeling study. *Adv. Water Resour.* **2010**, *33*, 1388–1401. [CrossRef]
14. Korol, A.R.; Noe, G.B. Patterns of Denitrification Potential in Tidal Freshwater Forested Wetlands. *Estuaries Coasts* **2020**, *43*, 329–346. [CrossRef]
15. Miao, G.; Noormets, A.; Domec, J.C.; Fuentes, M.; Trettin, C.C.; Sun, G.; McNulty, S.G.; King, J.S. Hydrology and microtopography control carbon dynamics in wetlands: Implications in partitioning ecosystem respiration in a coastal plain forested wetland. *Agric. For. Meteorol.* **2017**, *247*, 343–355. [CrossRef]
16. Trettin, C.C.; Czwartacki, B.J.; Allan, C.J.; Amatya, D.M. Linking freshwater tidal hydrology to carbon cycling in bottomland hardwood wetlands. In *Headwaters to Estuaries: Advances in Watershed Science and Management*; Stringer, C.E., Krauss, K.W., Latimer, J.S., Eds.; US Department of Agriculture Forest Service, Southern Research Station: Asheville, NC, USA, 2016; 302p.
17. Eppinga, M.B.; de Ruiter, P.C.; Wassen, M.J.; Rietkerk, M. Nutrients and hydrology indicate the driving mechanisms of peatland surface patterning. *Am. Nat.* **2009**, *173*, 803–818. [CrossRef] [PubMed]

18. Frei, S.; Knorr, K.H.; Peiffer, S.; Fleckenstein, J.H. Surface micro-topography causes hot spots of biogeochemical activity in wetland systems: A virtual modeling experiment. *J. Geophys. Res.* **2012**, *117*. [CrossRef]
19. Yamashita, N.; Ishizuka, S.; Hashimoto, S.; Ugawa, S.; Nanko, K.; Osone, Y.; Iwahashi, J.; Sakai, Y.; Inatomi, M.; Kawanishi, A.; et al. National-scale 3D mapping of soil organic carbon in a Japanese forest considering microtopography and tephra deposition. *Geoderma* **2022**, *406*, 115534. [CrossRef]
20. Huenneke, L.F.; Sharitz, R.R. Microsite Abundance and Distribution of Woody Seedlings in a South Carolina Cypress-Tupelo Swamp. *Am. Midl. Nat.* **1986**, *115*, 328–335. [CrossRef]
21. Titus, J.H. Microtopography and Woody Plant Regeneration in a Hardwood Floodplain Swamp in Florida. *Bull. Torrey Bot. Club* **1990**, *117*, 429–437. [CrossRef]
22. Bledsoe, B.P.; Shear, T.H. Vegetation along hydrologic and edaphic gradients in a North Carolina coastal plain creek bottom and implications for restoration. *Wetlands* **2000**, *20*, 126–147. [CrossRef]
23. Moser, K.; Ahn, C.; Noe, G. Characterization of microtopography and its influence on vegetation patterns in created wetlands. *Wetlands* **2007**, *27*, 1081–1097. [CrossRef]
24. Diamond, J.S.; Epstein, J.M.; Cohen, M.J.; McLaughlin, D.L.; Hsueh, Y.; Keim, R.F.; Duberstein, J.A. A little relief: Ecological functions and autogenesis of wetland microtopography. *Wiley Interdiscip. Rev. Water* **2021**, *8*, e1493. [CrossRef]
25. Stovall, A.E.L.; Diamond, J.S.; Slesak, R.A.; McLaughlin, D.L.; Shugart, H. Quantifying wetland microtopography with terrestrial laser scanning. *Remote Sens. Environ.* **2019**, *232*, 111271. [CrossRef]
26. Baltensweiler, A.; Heuvelink, G.B.M.; Hanewinkel, M.; Walthert, L. Microtopography shapes soil pH in flysch regions across Switzerland. *Geoderma* **2020**, *380*, 114663. [CrossRef]
27. Diamond, J.S.; McLaughlin, D.L.; Slesak, R.A.; Stovall, A. Pattern and structure of microtopography implies autogenic origins in forested wetlands. *Hydrol. Earth Syst. Sci.* **2019**, *23*, 5069–5088. [CrossRef]
28. Strack, M.; Waddington, J.M.; Rochefort, L.; Tuittila, E.S. Response of vegetation and net ecosystem carbon dioxide exchange at different peatland microforms following water table drawdown. *J. Geophys. Res.* **2006**, *111*. [CrossRef]
29. Xie, X.; Li, A.; Tian, J.; Wu, C.; Jin, H. A fine spatial resolution estimation scheme for large-scale gross primary productivity (GPP) in mountain ecosystems by integrating an eco-hydrological model with the combination of linear and non-linear downscaling processes. *J. Hydrol.* **2023**, *616*, 128833. [CrossRef]
30. Nouwakpo, S.K.; Weltz, M.A.; McGwire, K.C.; Williams, J.C.; Osama, A.H.; Green, C.H.M. Insight into sediment transport processes on saline rangeland hillslopes using three-dimensional soil microtopography changes. *Earth Surf. Process. Landforms* **2017**, *42*, 681–696. [CrossRef]
31. Williams, C.J.; Pierson, F.B.; Robichaud, P.R.; Al-Hamdan, O.Z.; Boll, J.; Strand, E.K. Structural and functional connectivity as a driver of hillslope erosion following disturbance. *Int. J. Wildland Fire* **2016**, *25*, 306. [CrossRef]
32. Diamond, J.S.; Mclaughlin, D.L.; Slesak, R.A.; Stovall, A. Microtopography is a fundamental organizing structure of vegetation and soil chemistry in black ash wetlands. *Biogeosciences* **2020**, *17*, 901–915. [CrossRef]
33. Graham, J.D.; Ricciuto, D.M.; Glenn, N.F.; Hanson, P.J. Incorporating microtopography in a land surface model and quantifying the effect on the carbon cycle. *J. Adv. Model. Earth Syst.* **2022**, *14*, e2021MS002721. [CrossRef]
34. Kalacska, M.; Arroyo-Mora, J.P.; Lucanus, O. Comparing UAS LiDAR and Structure-from-Motion Photogrammetry for Peatland Mapping and Virtual Reality (VR) Visualization. *Drones* **2021**, *5*, 36. [CrossRef]
35. Moore, P.A.; Lukenbach, M.C.; Thompson, D.K.; Kettridge, N.; Granath, G.; Waddington, J.M. Assessing the peatland hummock–hollow classification framework using high-resolution elevation models: implications for appropriate complexity ecosystem modeling. *Biogeosciences* **2019**, *16*, 3491–3506. [CrossRef]
36. Johnson, C.E.; Ruiz-Méndez, J.J.; Lawrence, G.B. Forest soil chemistry and terrain attributes in a Catskills watershed. *Soil Sci. Soc. Am. J.* **2000**, *64*, 1804–1814. [CrossRef]
37. Brubaker, K.M.; Myers, W.L.; Drohan, P.J.; Miller, D.A.; Boyer, E.W. The Use of LiDAR Terrain Data in Characterizing Surface Roughness and Microtopography. *Appl. Environ. Soil Sci.* **2013**, *2013*, 891534. [CrossRef]
38. Mercer, J.J.; Westbrook, C.J. Ultrahigh-resolution mapping of peatland microform using ground-based structure from motion with multiview stereo. *J. Geophys. Res. Biogeosci.* **2016**, *121*, 2901–2916. [CrossRef]
39. Knight, J.M.; Dale, P.E.R.; Spencer, J.; Griffin, L. Exploring LiDAR data for mapping the micro-topography and tidal hydrodynamics of mangrove systems: An example from southeast Queensland, Australia. *Estuar. Coast. Shelf Sci.* **2009**, *85*, 593–600. [CrossRef]
40. Rodríguez-Caballero, E.; Cantón, Y.; Chamizo, S.; Lázaro, R.; Escudero, A. Soil Loss and Runoff in Semiarid Ecosystems: A Complex Interaction Between Biological Soil Crusts, Micro-topography, and Hydrological Drivers. *Ecosystems* **2013**, *16*, 529–546. [CrossRef]
41. Brecheisen, Z.S.; Richter, D.D. Gully-erosion estimation and terrain reconstruction using analyses of microtopographic roughness and LiDAR. *Catena* **2021**, *202*, 105264. [CrossRef]
42. Siewert, M.B.; Hanisch, J.; Weiss, N.; Kuhry, P.; Maximov, T.C.; Hugelius, G. Comparing carbon storage of Siberian tundra and taiga permafrost ecosystems at very high spatial resolution. *J. Geophys. Res. Biogeosci.* **2015**, *120*, 1973–1994. [CrossRef]
43. Smith, M.W.; Warburton, J. Microtopography of bare peat: a conceptual model and objective classification from high-resolution topographic survey data. *Earth Surf. Process. Landforms* **2018**, *43*, 1557–1574. [CrossRef]

44. Davidson, S.J.; Santos, M.J.; Sloan, V.L.; Reuss-Schmidt, K.; Phoenix, G.K.; Oechel, W.C.; Zona, D. Upscaling CH4 Fluxes Using High-Resolution Imagery in Arctic Tundra Ecosystems. *Remote Sens.* **2017**, *9*, 1227. [CrossRef]
45. Bisht, G.; Riley, W.J.; Wainwright, H.M.; Dafflon, B.; Yuan, F.; Romanovsky, V.E. Impacts of microtopographic snow redistribution and lateral subsurface processes on hydrologic and thermal states in an Arctic polygonal ground ecosystem: a case study using ELM-3D v1.0. *Geosci. Model Dev.* **2018**, *11*, 61–76. [CrossRef]
46. Jan, A.; Coon, E.T.; Graham, J.D.; Painter, S.L. A Subgrid Approach for Modeling Microtopography Effects on Overland Flow. *Water Resources Research* **2018**, *54*, 6153–6167. [CrossRef]
47. Abolt, C.J.; Young, M.H. High-resolution mapping of spatial heterogeneity in ice wedge polygon geomorphology near Prudhoe Bay, Alaska. *Sci. Data* **2020**, *7*, 87. [CrossRef]
48. Falco, N.; Wainwright, H.; Dafflon, B.; Léger, E.; Peterson, J.; Steltzer, H.; Wilmer, C.; Rowland, J.C.; Williams, K.H.; Hubbard, S.S. Investigating microtopographic and soil controls on a mountainous meadow plant community using high-resolution remote sensing and surface geophysical data. *J. Geophys. Res. Biogeosci.* **2019**, *124*, 1618–1636. [CrossRef]
49. Solórzano, J.V.; Gallardo-Cruz, J.A.; Peralta-Carreta, C.; Martínez-Camilo, R.; de Oca, A.F.M. Plant community composition patterns in relation to microtopography and distance to water bodies in a tropical forested wetland. *Aquat. Bot.* **2020**, *167*, 103295. [CrossRef]
50. Alexander, C.; Deák, B.; Heilmeier, H. Micro-topography driven vegetation patterns in open mosaic landscapes. *Ecol. Indic.* **2016**, *60*, 906–920. [CrossRef]
51. Alexander, C.; Korstjens, A.H.; Hill, R.A. Influence of micro-topography and crown characteristics on tree height estimations in tropical forests based on LiDAR canopy height models. *Int. J. Appl. Earth Obs. Geoinf.* **2018**, *65*, 105–113. [CrossRef]
52. Harris, A.; Baird, A.J. Microtopographic drivers of vegetation patterning in blanket peatlands recovering from erosion. *Ecosystems* **2019**, *22*, 1035–1054. [CrossRef]
53. Devadoss, J.; Falco, N.; Dafflon, B.; Wu, Y.; Franklin, M.; Hermes, A.; Hinckley, E.L.S.; Wainwright, H. Remote Sensing-Informed Zonation for Understanding Snow, Plant and Soil Moisture Dynamics within a Mountain Ecosystem. *Remote Sens.* **2020**, *12*, 2733. [CrossRef]
54. Leong, R.C.; Friess, D.A.; Crase, B.; Lee, W.K.; Webb, E.L. High-resolution pattern of mangrove species distribution is controlled by surface elevation. *Estuar. Coast. Shelf Sci.* **2018**, *202*, 185–192. [CrossRef]
55. Wainwright, H.M.; Oktem, R.; Dafflon, B.; Dengel, S.; Curtis, J.B.; Torn, M.S.; Cherry, J.; Hubbard, S.S. High-Resolution Spatio-Temporal Estimation of Net Ecosystem Exchange in Ice-Wedge Polygon Tundra Using In Situ Sensors and Remote Sensing Data. *Land* **2021**, *10*, 722. [CrossRef]
56. Yelenik, S.; Rose, E.; Cordell, S.; Victoria, M.; Kellner, J.R. The role of microtopography and resident species in post-disturbance recovery of arid habitats in Hawai'i. *Ecol. Appl.* **2022**, *32*, e2690. [CrossRef] [PubMed]
57. Parker, A.F.; Owens, P.R.; Libohova, Z.; Wu, X.B.; Wilding, L.P.; Archer, S.R. Use of terrain attributes as a tool to explore the interaction of vertic soils and surface hydrology in South Texas playa wetland systems. *J. Arid Environ.* **2010**, *74*, 1487–1493. [CrossRef]
58. Lee, C.F.; Huang, W.K.; Chang, Y.L.; Chi, S.Y.; Liao, W.C. Regional landslide susceptibility assessment using multi-stage remote sensing data along the coastal range highway in northeastern Taiwan. *Geomorphology* **2018**, *300*, 113–127. [CrossRef]
59. Azarafza, M.; Azarafza, M.; Akgün, H.; Atkinson, P.M.; Derakhshani, R. Deep learning-based landslide susceptibility mapping. *Sci. Rep.* **2021**, *11*, 24112. [CrossRef] [PubMed]
60. Pawłuszek, K.; Borkowski, A.; Tarolli, P. Towards the optimal pixel size of Dem for automatic mapping of landslide areas. *ISPRS—Int. Arch. Photogramm. Remote Sens. Spat. Inf. Sci.* **2017**, *XLII-1/W1*, 83–90. [CrossRef]
61. Martínez Prentice, R.; Villoslada Peciña, M.; Ward, R.D.; Bergamo, T.F.; Joyce, C.B.; Sepp, K. Machine Learning Classification and Accuracy Assessment from High-Resolution Images of Coastal Wetlands. *Remote Sens.* **2021**, *13*, 3669. [CrossRef]
62. Turner, M.G. Landscape ecology: What is the state of the science? *Annu. Rev. Ecol. Evol. Syst.* **2005**, *36*, 319–344. [CrossRef]
63. Bian, L. Multiscale Nature of Spatial Data in Scaling Up Environmental Models, 2023. Available online: https://www.taylorfrancis.com/chapters/edit/10.1201/9780203740170-2/multiscale-nature-spatial-data-scaling-environmental-models-ling-bian (accessed on 10 January 2023).
64. Lam, N.S.N.; Quattrochi, D.A. On the Issues of Scale, Resolution, and Fractal Analysis in the Mapping Sciences. *Prof. Geogr.* **1992**, *44*, 88–98. [CrossRef]
65. Baltensweiler, A.; Walthert, L.; Ginzler, C.; Sutter, F.; Purves, R.S.; Hanewinkel, M. Terrestrial laser scanning improves digital elevation models and topsoil pH modelling in regions with complex topography and dense vegetation. *Environ. Model. Softw.* **2017**, *95*, 13–21. [CrossRef]
66. Habtezion, N.; Tahmasebi Nasab, M.; Chu, X. How does DEM resolution affect microtopographic characteristics, hydrologic connectivity, and modelling of hydrologic processes? *Hydrol. Process.* **2016**, *30*, 4870–4892. [CrossRef]
67. Lindsay, J.B. Whitebox GAT: A case study in geomorphometric analysis. *Comput. Geosci.* **2016**, *95*, 75–84. [CrossRef]
68. Minick, K.J.; Kelley, A.M.; Miao, G.; Li, X.; Noormets, A.; Mitra, B.; King, J.S. Microtopography alters hydrology, phenol oxidase activity and nutrient availability in organic soils of a coastal freshwater forested wetland. *Wetlands* **2019**, *39*, 263–273. [CrossRef]
69. Pérez-Ceballos.; Echeverría-Ávila.; Zaldivar-Jimenez, A.; Zaldivar-Jimenez, T.; Herrera-Silveira, J. Contribution of microtopography and hydroperiod to the natural regeneration of Avicennia germinans in a restored mangrove forest. *Cienc. Mar.* **2017**, *43*, 55–67. [CrossRef]

70. Wang, M.; Han, Y.; Xu, Z.; Wang, S.; Jiang, M.; Wang, G. Hummock-hollow microtopography affects soil enzyme activity by creating environmental heterogeneity in the sedge-dominated peatlands of the Changbai Mountains, China. *Ecol. Indic.* **2021**, *121*, 107187. [CrossRef]
71. Hardin, P.J.; Lulla, V.; Jensen, R.R.; Jensen, J.R. Small Unmanned Aerial Systems (sUAS) for environmental remote sensing: challenges and opportunities revisited. *GISci. Remote Sens.* **2019**, *56*, 309–322. [CrossRef]
72. Tang, W.; Chen, S.E.; Diemer, J.; Allan, C.; Chen, T.; Slocum, Z.; Shukla, T.; Chavan, V.S.; Shanmugam, N.S. *DeepHyd: A Deep Learning-Based Artificial Intelligence Approach for the Automated Classification of Hydraulic Structures from LiDAR and Sonar Data*; Technical Report FHWA/NC/2019-03; Dept. of Geography and Earth Sciences, University of North Carolina at Charlotte: Charlotte, NC, USA, 2022.
73. Hodgson, M.E.; Bresnahan, P. Accuracy of airborne lidar-derived elevation: Empirical assessment and error budget. *Photogramm. Eng. Remote Sens.* **2002**, *70*, 331–340. [CrossRef]
74. Pinton, D.; Canestrelli, A.; Wilkinson, B.; Ifju, P.; Ortega, A. Estimating Ground Elevation and Vegetation Characteristics in Coastal Salt Marshes Using UAV-Based LiDAR and Digital Aerial Photogrammetry. *Remote Sens.* **2021**, *13*, 4506. [CrossRef]
75. Almquist, B.; Jack, S.B.; Messina, M.G. Variation of the treefall gap regime in a bottomland hardwood forest: relationships with microtopography. *For. Ecol. Manage* **2002**, *157*, 155–163. [CrossRef]
76. Koponen, P.; Nygren, P.; Sabatier, D.; Rousteau, A.; Saur, E. Tree species diversity and forest structure in relation to microtopography in a tropical freshwater swamp forest in French Guiana. *Plant Ecol.* **2004**, *173*, 17–32. [CrossRef]
77. Agraz Hernández, C.M.; García Zaragoza, C.; Iriarte-Vivar, S.; Flores-Verdugo, F.J.; Moreno Casasola, P. Forest structure, productivity and species phenology of mangroves in the La Mancha lagoon in the Atlantic coast of Mexico. *Wetlands Ecol. Manage* **2011**, *19*, 273–293. [CrossRef]
78. Lucieer, A.; Turner, D.; King, D.H.; Robinson, S.A. Using an Unmanned Aerial Vehicle (UAV) to capture micro-topography of Antarctic moss beds. *Int. J. Appl. Earth Obs. Geoinf.* **2014**, *27*, 53–62. [CrossRef]
79. Lovitt, J.; Rahman, M.M.; Saraswati, S.; McDermid, G.J.; Strack, M.; Xu, B. UAV remote sensing can reveal the effects of low-impact seismic lines on surface morphology, hydrology, and methane (CH4) release in a boreal treed bog. *J. Geophys. Res. Biogeosci.* **2018**, *123*, 1117–1129. [CrossRef]
80. Kelly, J.; Kljun, N.; Eklundh, L.; Klemedtsson, L.; Liljebladh, B.; Olsson, P.O.; Weslien, P.; Xie, X. Modelling and upscaling ecosystem respiration using thermal cameras and UAVs: Application to a peatland during and after a hot drought. *Agric. For. Meteorol.* **2021**, *300*, 108330. [CrossRef]
81. Nouwakpo, S.K.; Weltz, M.A.; McGwire, K. Assessing the performance of structure-from-motion photogrammetry and terrestrial LiDAR for reconstructing soil surface microtopography of naturally vegetated plots. *Earth Surf. Process. Landforms* **2016**, *41*, 308–322. [CrossRef]
82. Lowe, D.G. Distinctive Image Features from Scale-Invariant Keypoints. *Int. J. Comput. Vis.* **2004**, *60*, 91–110. [CrossRef]
83. Becker, T.; Kutzbach, L.; Forbrich, I.; Schneider, J.; Jager, D.; Thees, B.; Wilmking, M. Do we miss the hot spots? – The use of very high resolution aerial photographs to quantify carbon fluxes in peatlands. *Biogeosciences* **2008**, *5*, 1387–1393. [CrossRef]
84. Lehmann, J.R.K.; Münchberger, W.; Knoth, C.; Blodau, C.; Nieberding, F.; Prinz, T.; Pancotto, V.A.; Kleinebecker, T. High-Resolution Classification of South Patagonian Peat Bog Microforms Reveals Potential Gaps in Up-Scaled CH4 Fluxes by use of Unmanned Aerial System (UAS) and CIR Imagery. *Remote Sens.* **2016**, *8*, 173. [CrossRef]
85. Jeziorska, J. UAS for Wetland Mapping and Hydrological Modeling. *Remote Sens.* **2019**, *11*, 1997. [CrossRef]
86. Mallet, C.; Bretar, F. Full-waveform topographic lidar: State-of-the-art. *ISPRS J. Photogramm. Remote Sens.* **2009**, *64*, 1–16. [CrossRef]
87. Chasmer, L.; Hopkinson, C.; Montgomery, J.; Petrone, R. A Physically Based Terrain Morphology and Vegetation Structural Classification for Wetlands of the Boreal Plains, Alberta, Canada. *Can. J. Remote Sens.* **2016**, *42*, 521–540. [CrossRef]
88. Lang, M.W.; Kim, V.; McCarty, G.W.; Li, X.; Yeo, I.Y.; Huang, C.; Du, L. Improved Detection of Inundation below the Forest Canopy using Normalized LiDAR Intensity Data. *Remote Sens.* **2020**, *12*, 707. [CrossRef]
89. Ward, R.D.; Burnside, N.G.; Joyce, C.B.; Sepp, K. The use of medium point density LiDAR elevation data to determine plant community types in Baltic coastal wetlands. *Ecol. Indic.* **2013**, *33*, 96–104. [CrossRef]
90. Hilker, T.; van Leeuwen, M.; Coops, N.C.; Wulder, M.A.; Newnham, G.J.; Jupp, D.L.B.; Culvenor, D.S. Comparing canopy metrics derived from terrestrial and airborne laser scanning in a Douglas-fir dominated forest stand. *Trees* **2010**, *24*, 819–832. [CrossRef]
91. Rodríguez-Caballero, E.; Afana, A.; Chamizo, S.; Solé-Benet, A.; Canton, Y. A new adaptive method to filter terrestrial laser scanner point clouds using morphological filters and spectral information to conserve surface micro-topography. *ISPRS J. Photogramm. Remote Sens.* **2016**, *117*, 141–148. [CrossRef]
92. Cianciolo, T.R.; Diamond, J.S.; McLaughlin, D.L.; Slesak, R.A.; D'Amato, A.W.; Palik, B.J. Hydrologic variability in black ash wetlands: Implications for vulnerability to emerald ash borer. *Hydrol. Process.* **2021**, *35*, e14014. [CrossRef]
93. Liao, C.; Li, H.; Lv, G.; Tian, J.; Xu, Y. Effects of ecological restoration on soil properties of the aeolian sandy land around Lhasa, southern Tibetan Plateau. *Ecosphere* **2020**, *11*, e03009. [CrossRef]
94. Rusu, R.B.; Cousins, S. 3D is here: Point Cloud Library (PCL). In Proceedings of the 2011 IEEE International Conference on Robotics and Automation, Shanghai, China, 9–13 May 2011; pp. 1–4.
95. Zhang, W.; Qi, J.; Wan, P.; Wang, H.; Xie, D.; Wang, X.; Yan, G. An Easy-to-Use Airborne LiDAR Data Filtering Method Based on Cloth Simulation. *Remote Sens.* **2016**, *8*, 501. [CrossRef]

96. Kalacska, M.; Chmura, G.L.; Lucanus, O.; Bérubé, D.; Arroyo-Mora, J.P. Structure from motion will revolutionize analyses of tidal wetland landscapes. *Remote Sens. Environ.* **2017**, *199*, 14–24. [CrossRef]
97. Griffin, L.F.; Knight, J.M.; Dale, P.E.R. Identifying mosquito habitat microtopography in an Australian mangrove forest using LiDAR derived elevation data. *Wetlands* **2010**, *30*, 929–937. [CrossRef]
98. Korpela, I.; Haapanen, R.; Korrensalo, A.; Tuittila, E.S.; Vesala, T. Fine-resolution mapping of microforms of a boreal bog using aerial images and waveform-recording LiDAR. *Mires Peat* **2020**, *26*, 2–25.
99. Anderson, K.; Bennie, J.; Wetherelt, A. Laser scanning of fine scale pattern along a hydrological gradient in a peatland ecosystem. *Landsc. Ecol.* **2010**, *25*, 477–492. [CrossRef]
100. Zhang, X.; Meng, X.; Li, C.; Shang, N.; Wang, J.; Xu, Y.; Wu, T.; Mugnier, C. Micro-Topography Mapping through Terrestrial LiDAR in Densely Vegetated Coastal Environments. *ISPRS Int. J. Geo-Inf.* **2021**, *10*, 665. [CrossRef]
101. Wang, Y.J.; Cheng-Zhi, Q.; A-Xing, Z. Review on algorithms of dealing with depressions in grid DEM. *Ann. GIS* **2019**, *25*, 83–97. [CrossRef]
102. Wu, Q.; Lane, C.R.; Wang, L.; Vanderhoof, M.K.; Christensen, J.R.; Liu, H. Efficient delineation of nested depression hierarchy in digital elevation models for hydrological analysis using level-set method. *J Am Water Resour Assoc.* **2019**, *55*, 354–368. [CrossRef] [PubMed]
103. Wang, L.; Liu, H. An efficient method for identifying and filling surface depressions in digital elevation models for hydrologic analysis and modelling. *Int. J. Geogr. Inf. Sci.* **2006**, *20*, 193–213. [CrossRef]
104. Wu, Q.; Lane, C.R. Delineation and quantification of wetland depressions in the prairie pothole region of North Dakota. *Wetlands* **2016**, *36*, 215–227. [CrossRef]
105. Wu, Q.; Lane, C.R. Delineating wetland catchments and modeling hydrologic connectivity using lidar data and aerial imagery. *Hydrol. Earth Syst. Sci.* **2017**, *21*, 3579–3595. [CrossRef] [PubMed]
106. Chu, X.; Yang, J.; Chi, Y.; Zhang, J. Dynamic puddle delineation and modeling of puddle-to-puddle filling-spilling-merging-splitting overland flow processes. *Water Resour. Res.* **2013**, *49*, 3825–3829. [CrossRef]
107. Abolt, C.J.; Young, M.H.; Atchley, A.L.; Wilson, C.J. Brief communication: Rapid machine-learning-based extraction and measurement of ice wedge polygons in high-resolution digital elevation models. *Cryosphere* **2019**, *13*, 237–245. [CrossRef]
108. Witharana, C.; Bhuiyan, M.A.E.; Liljedahl, A.K.; Kanevskiy, M.; Epstein, H.E.; Jones, B.M.; Daanen, R.; Griffin, C.G.; Kent, K.; Ward Jones, M.K. Understanding the synergies of deep learning and data fusion of multispectral and panchromatic high resolution commercial satellite imagery for automated ice-wedge polygon detection. *ISPRS J. Photogramm. Remote Sens.* **2020**, *170*, 174–191. [CrossRef]
109. LeCun, Y.; Bengio, Y.; Hinton, G. Deep learning. *Nature* **2015**, *521*, 436–444. [CrossRef]
110. Huang, L.; Liu, L.; Jiang, L.; Zhang, T. Automatic Mapping of Thermokarst Landforms from Remote Sensing Images Using Deep Learning: A Case Study in the Northeastern Tibetan Plateau. *Remote Sens.* **2018**, *10*, 2067. [CrossRef]
111. Brooks, R.T.; Hayashi, M. Depth-area-volume and hydroperiod relationships of ephemeral (vernal) forest pools in southern New England. *Wetlands* **2002**, *22*, 247–255. [CrossRef]
112. Gamble, D.L.; Mitsch, W.J. Hydroperiods of created and natural vernal pools in central Ohio: A comparison of depth and duration of inundation. *Wetlands Ecol. Manage* **2009**, *17*, 385–395. [CrossRef]
113. Hesselbarth, M.H.K.; Sciaini, M.; With, K.A.; Wiegand, K.; Nowosad, J. landscapemetrics : an open-source R tool to calculate landscape metrics. *Ecography* **2019**, *42*, 1648–1657. [CrossRef]
114. Congalton, R.G. A review of assessing the accuracy of classifications of remotely sensed data. *Remote Sens. Environ.* **1991**, *37*, 35–46. [CrossRef]
115. Liu, C.; Frazier, P.; Kumar, L. Comparative assessment of the measures of thematic classification accuracy. *Remote Sens. Environ.* **2007**, *107*, 606–616. [CrossRef]
116. Cavallaro, N.; Shrestha, G.; Birdsey, R.; Mayes, M.A.; Najjar, R.G.; Reed, S.C.; Romero-Lankao, P.; Zhu, Z. *Second State of the Carbon Cycle Report (SOCCR2): A sustained Assessment Report*; Technical report; 2018. Available online: https://carbon2018.globalchange.gov/ (accessed on 10 January 2023).
117. Shi, X.; Thornton, P.E.; Ricciuto, D.M.; Hanson, P.J.; Mao, J.; Sebestyen, S.D.; Griffiths, N.A.; Bisht, G. Representing northern peatland microtopography and hydrology within the Community Land Model. *Biogeosciences* **2015**, *12*, 6463–6477. [CrossRef]
118. Padró, J.C.; Muñoz, F.J.; Planas, J.; Pons, X. Comparison of four UAV georeferencing methods for environmental monitoring purposes focusing on the combined use with airborne and satellite remote sensing platforms. *Int. J. Appl. Earth Obs. Geoinf.* **2019**, *75*, 130–140. [CrossRef]
119. Pinheiro, M.; Reigber, A.; Scheiber, R.; Prats-Iraola, P.; Moreira, A. Generation of Highly Accurate DEMs Over Flat Areas by Means of Dual-Frequency and Dual-Baseline Airborne SAR Interferometry. *IEEE Trans. Geosci. Remote Sens.* **2018**, *56*, 4361–4390. [CrossRef]
120. Choi, C.; Kim, D.J. Optimum Baseline of a Single-Pass In-SAR System to Generate the Best DEM in Tidal Flats. *IEEE J. Sel. Top. Appl. Earth Obs. Remote Sens.* **2018**, *11*, 919–929. [CrossRef]
121. Budei, B.C.; St-Onge, B.; Hopkinson, C.; Audet, F.A. Identifying the genus or species of individual trees using a three-wavelength airborne lidar system. *Remote Sens. Environ.* **2018**, *204*, 632–647. [CrossRef]
122. Hopkinson, C.; Chasmer, L.; Gynan, C.; Mahoney, C.; Sitar, M. Multisensor and Multispectral LiDAR Characterization and Classification of a Forest Environment. *Can. J. Remote Sens.* **2016**, *42*, 501–520. [CrossRef]

123. Yu, X.; Hyyppä, J.; Litkey, P.; Kaartinen, H.; Vastaranta, M.; Holopainen, M. Single-sensor solution to tree species classification using multispectral airborne laser scanning. *Remote Sens.* **2017**, *9*, 108. [CrossRef]
124. Li, X.; Liu, C.; Wang, Z.; Xie, X.; Li, D.; Xu, L. Airborne LiDAR: state-of-the-art of system design, technology and application. *Meas. Sci. Technol.* **2020**, *32*, 032002. [CrossRef]
125. Panagou, T.; Oikonomou, E.; Hasiotis, T.; Velegrakis, A.F. Shallow Water Bathymetry Derived from Green Wavelength Terrestrial Laser Scanner. *Mar. Geod.* **2020**, *43*, 472–492. [CrossRef]
126. Guo, X.; Yan, X.; Zheng, S.; Wang, H.; Yin, P. Characteristics of high-resolution subaqueous micro-topography in the Jinshan Deep Trough and its implications for riverbed deformation, Hangzhou Bay, China. *Estuar. Coast. Shelf Sci.* **2021**, *250*, 107147. [CrossRef]
127. Manyika, J.; Chui, M.; Brown, B.; Bughin, J.; Dobbs, R.; Roxburgh, C.; Hung Byers, A. *Big Data: The Next Frontier for Innovation, Competition, and Productivity*; McKinsey Global Institute: 2011. Available online: https://www.mckinsey.com/capabilities/mckinsey-digital/our-insights/big-data-the-next-frontier-for-innovation (accessed on 10 January 2023).
128. Tang, W.; Shaowen, W. *High Performance Computing for Geospatial Applications*; Springer International Publishing: Berlin/Heidelberg, Germany, 2020; Chapter 4, pp. 53–76.
129. Zheng, M.; Tang, W.; Lan, Y.; Zhao, X.; Jia, M.; Allan, C.; Trettin, C. Parallel Generation of Very High Resolution Digital Elevation Models: High-Performance Computing for Big Spatial Data Analysis. *Big Data Eng. Appl.* **2018**, 21–39.
130. Barnes, R. Parallel Priority-Flood depression filling for trillion cell digital elevation models on desktops or clusters. *Comput. Geosci.* **2016**, *96*, 56–68. [CrossRef]


**Disclaimer/Publisher's Note:** The statements, opinions and data contained in all publications are solely those of the individual author(s) and contributor(s) and not of MDPI and/or the editor(s). MDPI and/or the editor(s) disclaim responsibility for any injury to people or property resulting from any ideas, methods, instructions or products referred to in the content.